





PAPER

[View Article Online](#)
[View Journal](#) | [View Issue](#)Cite this: *Dalton Trans.*, 2025, **54**, 11207**In(III) complexes of sulfonyldithiocarbimates as selective antineoplastic agents against human colorectal adenocarcinoma†**Lucas Raposo Carvalho, *^{†a} Aline de Souza Bozzi, *^{†b} Wanessa Maria Alves Faria,^a Lucas Gil Venturelli,^a Túlio Duque Esteves,^a Sâmia Sousa Duarte,^c Ramon Ramos Marques de Souza,^c Isione Oliveira Castro,^c Eclair Venturini Filho,^d Renata Diniz, ^e Marianna Vieira Sobral,^c Willian Ricardo Rocha ^b and Eder do Couto Tavares^a

The synthesis, antineoplastic profile, and structural aspects of six In(III) sulfonyldithiocarbimate complexes ($\text{Ph}_4\text{P}[(\text{RSO}_2\text{N}=\text{CS}_2)_2\text{In}]$, **2a–f**) are described. The salts were readily obtainable with 38% to 98% yield by the water-mediated complexation of the ligand (**1a–f**) in the presence of $\text{In}(\text{NO}_3)_3$ without further purification. Spectroscopic data pointed to the formation of isomers, which were postulated as the result of three complexation modes – SS–SS, SN–SN, and SN–SS. DFT calculations furnished ΔG , K_{eq} , and δ values that indicated a preference for the SS–SS isomer. Statistical analysis of ^{13}C NMR data placed $^{13}\text{C}=\text{N}$ δ values as efficient probes of the d-electron count of the metal in sulfonyldithiocarbimate complexes. The compounds displayed antineoplastic activity against human colorectal adenocarcinoma (HCT-116) cell lines ($\text{IC}_{50} = 3.02(21) \mu\text{mol L}^{-1}$ to $5.36(42) \mu\text{mol L}^{-1}$) with high selectivity compared to HaCaT cells. Moreover, an XRD analysis of a water-insoluble decomposition product of a ligand (**1b**) is also described, showing the formation of a supramolecular-like network and corroborating the use of the metallic complexes as biologically active compounds instead of their isolated ligands.

Received 14th April 2025,
Accepted 30th June 2025

DOI: 10.1039/d5dt00868a

rsc.li/dalton**1. Introduction**

Alkylating agents are chemotherapeutic drugs that modify the DNA of cancer cells, preventing replication and inducing cell death. They are among the oldest antineoplastic drugs and

remain widely used in clinical practice.¹ In this context, platinum-based coordination complexes, such as cisplatin, carboplatin, and oxaliplatin, are highly effective due to their ability to form DNA cross-links, inhibiting replication and transcription, leading to programmed cell death.²

Approved for clinical use in 1978, cisplatin has been used for the treatment of numerous human cancers, including ovarian, testicular, lung, and colorectal cancer.³ At the same time, carboplatin is mainly used for ovarian cancer therapy but also exhibits antineoplastic activity in testis, cervical, neck, head, and small cell lung carcinoma.⁴ Regarding oxaliplatin, this drug is commonly used as a combination therapy with other chemotherapeutic agents, part of the FOLFOX regimen (5-fluorouracil, leucovorin, and oxaliplatin), mainly in the treatment of colon cancer and non-small-cell lung cancer.⁵ Despite their effectiveness, platinum-based therapies are associated with significant side effects, including nephrotoxicity, neurotoxicity, and acquired tumor resistance.^{5,6}

To overcome these limitations, research into new metal-based complexes has intensified. Compounds containing copper, gold, and indium have emerged as promising alternatives, demonstrated selective cytotoxicity, and reduced systemic toxicity.^{7–9} Recent studies suggest that indium-based com-

^aLaboratório Curie de Síntese, LaCSin, Instituto de Física e Química, Universidade Federal de Itajubá (UNIFEI), Avenida BPS, 1303, Pinheirinho, 37500-903 Itajubá, MG, Brazil. E-mail: lucas.raposo.c@gmail.com

^bLaboratório de Estudos Computacionais em Sistemas Moleculares, eCsMolab, Departamento de Química, ICEx, Universidade Federal de Minas Gerais (UFMG), 31270-901 Pampulha, Belo Horizonte, MG, Brazil. E-mail: alinedsbozzi@gmail.com

^cLaboratório de Oncofarmacologia, Departamento de Ciências Farmacêuticas, Universidade Federal de Paraíba (UFPB), Jardim Cidade Universitária, s/n, Castelo Branco, 58051-970 João Pessoa, PB, Brazil

^dCentro Universitário Salesiano (UniSales), Avenida Vitória 950, Forte São João, CEP 29017-950 Vitória, ES, Brazil

^eDepartamento de Química, ICEx, Universidade Federal de Minas Gerais (UFMG), 31270-901 Pampulha, Belo Horizonte, MG, Brazil

†Electronic supplementary information (ESI) available: (i) Experimental procedures, (ii) HRMS and NMR spectra, (iii) optimized atom coordinates, (iv) calculated chemical shifts, (v) HOMO plots, (vi) cytotoxicity plots, and (vii) selected geometric parameters. CCDC 2433188. For ESI and crystallographic data in CIF or other electronic format see DOI: <https://doi.org/10.1039/d5dt00868a>

‡These authors contributed equally to this work and share first authorship.

pounds can inhibit cancer cell growth and induce apoptosis, representing a promising therapeutic alternative for colorectal cancer treatment and other malignancies.^{10,11}

Notably, the literature on dithiocarbamates and their metallic complexes is quite vast. For instance, the cytotoxic activities of Pt(II), Mn(II), Cu(II), Zn(II), Cd(II), Bi(III), and many other metallic dithiocarbamate complexes were evaluated against human cervical adenocarcinoma (HeLa), human fetal lung cancer (MRC5-SV2), human cervical cancer (HeLa), and human adenocarcinoma (MCF-7) cell lines.^{12–15} However, to our knowledge, the only evaluation of metallic dithiocarbamate complexes for antitumoral-related applications in the literature is the study conducted by Castro *et al.*¹⁶ This study describes the interaction between two dithiocarbamate Pt(II) complexes and biotin-labeled γ -DNA and determined their modes of association. No patent documents about biological applications of dithiocarbamate-based metal complexes were found (detailed description of the patent database search is described in the ESI†). Therefore, this study brings much-needed data on novel avenues for antitumoral drug development based on these compounds.

Hence, this paper describes the synthesis and evaluation of six novel In(III) homoleptic sulfonyldithiocarbamate complexes and their cytotoxicity against MCF-7 (breast adenocarcinoma), SK-MEL-28 (human melanoma), and HCT-116 (colorectal adenocarcinoma) cell lines. Moreover, an extensive chemical, spectroscopical, and computational description is presented, shedding light on some crucial structural and biological properties of this incipient chemical system.

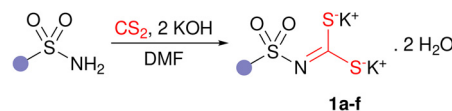
2. Results and discussion

2.1. Synthesis and characterization

Six potassium *N*-R-sulfonyldithiocarbamate dihydrate salts (**1a–f**), with general formula $K_2(R-SO_2N=CS_2) \cdot 2H_2O$, where $R = CH_3$ (**1a**), C_6H_5 (**1b**), $4-FC_6H_4$ (**1c**), $4-ClC_6H_4$ (**1d**), $4-BrC_6H_4$ (**1e**), and $4-IC_6H_4$ (**1f**) were prepared from the respective primary sulfonamides in a reaction with 1.5 molar eq. of carbon disulfide (CS_2) and 2 molar eq. of potassium hydroxide (KOH) in *N,N*-dimethylformamide (DMF), as shown in Fig. 1, following synthetic procedures adapted from ones described in the literature.^{17–19} The products were obtained as yellow solids, thoroughly water-soluble, and insoluble in organic solvents such as DMF and acetone.

A substantial difference between the adopted method and those described in the literature^{17–19} was the stepwise addition of KOH. Instead of adding both molar equivalents simultaneously, the appropriate mass was added in two portions and *ca.* one hour apart. Considering the base was used in a powder form, this addition method prevented clumping during the process and favored higher yields. Compound **1c** was synthesized using drops of DMF – enough to dissolve all reagents – instead of a larger volume, which is the condition used in the literature, so that the solubility of **1c** would not be compromised. This adaptation elevated the yield from 22% to

1. Base-mediated formation of potassium dithiocarbamates **1a–f**



2. Formation of complexes **2a–f** with In(III) and precipitation with PPh_4Cl

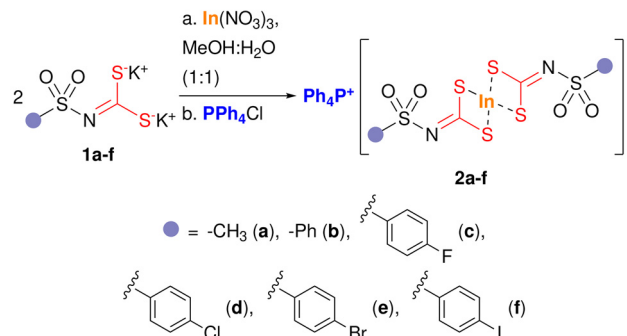


Fig. 1 Preparation of the potassium *N*-R-sulfonyldithiocarbamates (**1a–f**) following subsequent complexation with $In(NO_3)_3$ and precipitation with PPh_4Cl , yielding In(III) complexes **2a–f**.

63% for **1c**. A noteworthy aspect of this reaction is that the product does not need column chromatography purification after the synthesis, and the process is operationally simple, furnishing the ligand in a single step.

The synthesis of compounds **1a–f** was confirmed by comparing FTIR (Fourier Transform Infrared Spectroscopy) data with the literature.^{20,21} Dithiocarbamate formation was mainly verified by the presence of two sharp bands at $1255.3(5.9) \text{ cm}^{-1}$ ($\nu \text{ C=N}$) and $967.2(16.4) \text{ cm}^{-1}$ ($\nu_{as} \text{ CS}_2$), and by the absence of two sharp bands at *ca.* 3400 cm^{-1} , attributed to ν_{as} and ν_s of the NH_2 group. The $\nu \text{ C=N}$ -related band was observed in lower wavenumbers than usual – *i.e.*, *ca.* 1600 cm^{-1} – given the electron delocalization-enabled high single bond character of the $C=N$ bond for **1a–f** (Fig. 2).

The subsequent complexation of **1a–f** was done with 1 molar eq. of $In(NO_3)_3$ and 2 molar eq. of the respective dithiocarbamate in a methanol:water 1:1 (v:v) solution, furnishing **2a–f** (Fig. 1) with 38% to 98% yield. The 1:2 proportion between the metal and the ligands was deemed favorable considering previous ITC (Isothermal Titration Calorimetry) results for bis-(*N*-ethylsulfonyldithiocarbamate)In(III).²² Moreover, replacing $In(NO_3)_3$ with $InCl_3$ was inconsequential yield- and

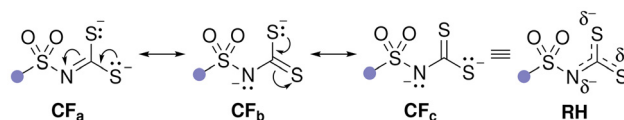


Fig. 2 Canonical forms (CF_i) and resonance hybrid (RH) of a general dithiocarbamate anion, representing the electronic delocalization, negative partial charges (δ^-), and the single bond character of the $C=N$ bond.

purity-wise. Considering that cost and ease of production are important aspects of the development of cancer-related medications,^{23,24} it is important to mention that the synthesis of **2a-f** involves a two-step synthetic procedure using mainly cheap reagents and no complicated purification steps.

Dithiocarbamate complexation and precipitation with Ph_4P^+ were attested by FTIR, HRMS (High-Resolution Mass Spectrometry), and NMR (Nuclear Magnetic Resonance) spectroscopy analyses. First, the band related to $\nu \text{C}=\text{N}$ underwent a hypsochromic shift to $1443.8(19.2) \text{ cm}^{-1}$, which is in line with other reported dithiocarbamate complexes.^{25,26} Accordingly, the band related to $\nu_{\text{as}} \text{CS}_2$ was bathochromically shifted to $951.2(16.6) \text{ cm}^{-1}$. Although the literature reports a more pronounced bathochromic shift – *i.e.*, to *ca.* 930 cm^{-1} (ref. 27 and 28) –, the spectra showed considerably wide bands in this region, which could indicate a superposition with bands at wavenumbers lower than 951.2 cm^{-1} . These shifts can be attributed to a greater double bond character to the $\text{C}=\text{N}$ bond in **2a-f** compared to **1a-f**, which is confirmed by the calculated wavenumber and bond order values for $\nu \text{C}=\text{N}$ of **1b** and **2b** (Table 1), chosen as model compounds.

The intermediate bond order for **1a** is adequately reflected by the lower calculated wavenumber for the $\nu \text{C}=\text{N}$ -related band. However, the calculated bond order and wavenumber increased after complexation. This can be rationalized by the more efficient conjugation for **1a-f** compared to **2a-f**, given the smaller energy gap between the filled sulfur nonbonding orbital (n_{S}^-) and the empty $\text{C}=\text{N}$ antibonding π orbital ($\pi^*_{\text{C}=\text{N}}$) for the latter. Complexation lowers the overall orbital energy of the dithiocarbamate portion, hindering conjugation and increasing the bond order. The same reasoning can be used to justify the hypsochromic shift of the $\nu_{\text{as}} \text{CS}_2$ band, considering the $\pi^*_{\text{C}=\text{S}}$ orbital instead of $\pi^*_{\text{C}=\text{N}}$.

The metallic complexes **2a-f** were submitted to HRMS analyses under ESI (electrospray ionization) in negative mode (Fig. S2†). All spectra showed peaks for the homoleptic complexes with a low relative error between calculated and observed values – *i.e.*, $0.39(35) \text{ ppm}$ –, indicating that the proposed molecular formulae are correct.²⁹

It is important to note that the literature shows instances of hexacoordinated In(III) dithiocarbamate complex.^{30,31} However, the In(III) complexes reported herein do not show this coordination pattern, adopting a tetracoordinated form, InL_2^- . De Freitas *et al.*²² attested to this preference with ITC data, showing a preference for 1 : 2 molar ratios and tetracoordination. Moreover, the HRMS analyses were conducted under soft ionization conditions, comparable to those reported by

Destefani *et al.* and Filho *et al.*^{29,32} In these conditions, neutral ligands remain coordinated to the metal center until data acquisition and are detected, suggesting a sufficiently gentle ionization process that preserves labile coordination interactions. No peaks corresponding to solvent- or water-coordinated species were observed in the acquired spectra (Fig. S2–S7†), even at low intensities. This absence of peaks supports the interpretation that such solvent molecules are not part of the coordination sphere in solution. Consequently, we propose that the InL_2^- species observed reflect the predominant coordination environment and are not the result of fragmentation under the experimental conditions. Finally, Fig. S2–S7† show an expansion of the HRMS spectrum of **2a-f** around the region corresponding to the possible addition of two coordinated water molecules in which no peak corresponding to the calculated spectrum can be observed.

Although HRMS analyses were instrumental in confirming the chemical identity of the reaction products as complexes **2a-f**, NMR analyses (Fig. S8–S19†) proved paramount in providing unambiguous structural characterization and understanding the system more intricately from a chemical standpoint.

First, the ^1H spectra for all compounds showed a slight excess of Ph_4P^+ given the relative integrals for its protons. Specifically, average cation : anion ^1H integral ratios, considering the specific proportions, ranged from 1.37(10) to 2.50(75) (Table S1†), showing a moderate cationic excess for all samples. Previous recrystallization attempts of an In(III) dithiocarbamate complex in methanol decomposed it into its corresponding dithiocarbamate, as attested by X-Ray Diffraction (XRD) analysis.²² Therefore, recrystallization is an unfeasible purification methodology for complexes **2a-f**.

Notably, the excess of Ph_4P^+ should not impact the biological assays, as suggested by some studies. The study conducted by Li *et al.* pertains to the antineoplastic activity of dysprosium thiocyanate complexes with Ph_4P^+ as the counterion.³³ The authors verified that the IC_{50} of Ph_4PBr were greater than $400 \mu\text{mol L}^{-1}$ for all cancer lines studies, including the human colorectal adenocarcinoma HT-29 cell line. Moreover, Thomadaki *et al.* researched the antineoplastic properties of 2,5-dihydroxybenzoate molybdenum(VI) complexes with Ph_4P^+ as the counterion against leukemia cell lines HL-60 and K562.³⁴ Comparison between the activities of the complexes and Ph_4PCl revealed that the phosphonium salt displayed negligible antineoplastic character. Hence, the cationic excess observed likely did not affect the outcome of the biological studies.

Second, the NMR analyses also showed the impact of diminishing electron delocalization from **1a-f** to **2a-f**. The ^{13}C -NMR spectra of dihydrate potassium dithiocarbamate salts – *i.e.*, $[\text{RSO}_2\text{N}=\text{CS}_2]\text{K}_2 \cdot 2\text{H}_2\text{O}$ – typically show a peak related to the $\text{C}=\text{N}$ carbon at *ca.* 225 ppm .^{26,35} In contrast, the spectra for dithiocarbamate-based metal complexes typically show a shielding effect for this carbon atom, shifting it to 200 ppm – 210 ppm ,^{26,35} which adequately reflects the values obtained in this work – *i.e.*, $207.5(2.81) \text{ ppm}$. This effect is often associated

Table 1 Calculated wavenumber (cm^{-1}) and Mayer bond order for $\nu \text{C}=\text{N}$ of **1b** and the SS–SS isomer of **2b**

Compound	Wavenumber (cm^{-1})	Mayer bond order
1b	1229.3	1.42
2b	1468.8 (ν_{S})	1.66
	1463.15 (ν_{as})	1.66

with a more significant contribution of the canonical form CF_c (Fig. 2) to the resonance hybrid (**H**, Fig. 2). However, a more accurate reasoning is given by analyzing the atomic partial charges for the $\text{C}=\text{N}$ carbon atom of **1b** and **2b**, obtained through calculations using CHELPG,³⁶ which were 0.53 and 0.28, respectively, reflecting a larger paramagnetic shielding (σ_{para}) after complexation, and contributing to a smaller isotropic chemical shift (δ_{iso}).³⁷

Another important aspect of this peak is the low signal-to-noise ratio (sino) of the $\text{C}=\text{N}$ peak for **2a–f**, which can be explained by its less pronounced intensification by the nOe, as was the case for C-4/C-4' and C-1/C-1', and by the low solubility of compounds **2a–f** in DMSO which, coupled to a smaller number of scans, can lead to a less intense signal. Moreover, it should be noted that quaternary ^{13}C signals have longer longitudinal relaxation times (T_1) given the lack of efficient ^1H – ^{13}C dipolar relaxation pathways, which was observed by Abdalrazaq *et al.* and Tan *et al.*^{14,38} Finally, considering that the $\text{C}=\text{N}$ carbon atom establishes a double bond to a quadrupolar ^{14}N atom, the scalar coupling between them could lead to smaller transverse relaxation times (T_2), broadening the signal and further lowering its intensity.

Third, the ^1H -NMR spectra of **2a–e** showed a noteworthy trend in the 7.0 ppm to 8.0 ppm region (Fig. 3). By maintaining the intensity of the Ph_4P^+ -related ^1H signals constant and analyzing the signals of H3/H5/H3'/H5' for compounds **2c–e**, a clear pattern was observed. While the neighboring triplet at *ca.*

7.3 ppm for **2c** – shown as the light gray region in Fig. 3 – had a negligible sino, the respective regions for compounds **2d** and **2e** displayed greater relative intensities. Given the similarity in their multiplicity pattern and their chemical shift proximity, these peaks are likely related to isomers of **2c–e**.

Since the ^{13}C -NMR spectra were acquired with power gated ^1H decoupling, the argument of signal intensity cannot be used. However, these spectra became considerably contaminated from **2b** to **2f** (Fig. S8–S19†), which indicated a proportional increase in isomer population. To address this, a theory for isomer formation was initially formulated. Considering the electron delocalization at the $\text{N}=\text{CS}_2^{2-}$ moiety of compounds **1a–f**, more than one coordination mode is possible, yielding three possible constitutional isomers for each complex (Fig. 4). One homoleptic isomer can be formed by the coordination of both dithiocarbimates using their sulfur atoms (SS–SS), another homoleptic isomer with each anion complexed by one sulfur and one nitrogen atom (SN–SN), and a heteroleptic isomer by the complexation of one dithiocarbimate with its sulfur atoms and the other with one sulfur and one nitrogen atom (SS–SN).

FTIR results could also attest to the formation of these isomers. Considering the previously discussed change in electron delocalization from **1a–f** to **2a–f**, one could argue that the SS-coordinated dithiocarbimate would have $\text{C}=\text{N}$ and $\text{C}-\text{S}$ bonds with a greater double and single bond character, respectively. In contrast, the SN-coordinated dithiocarbimate

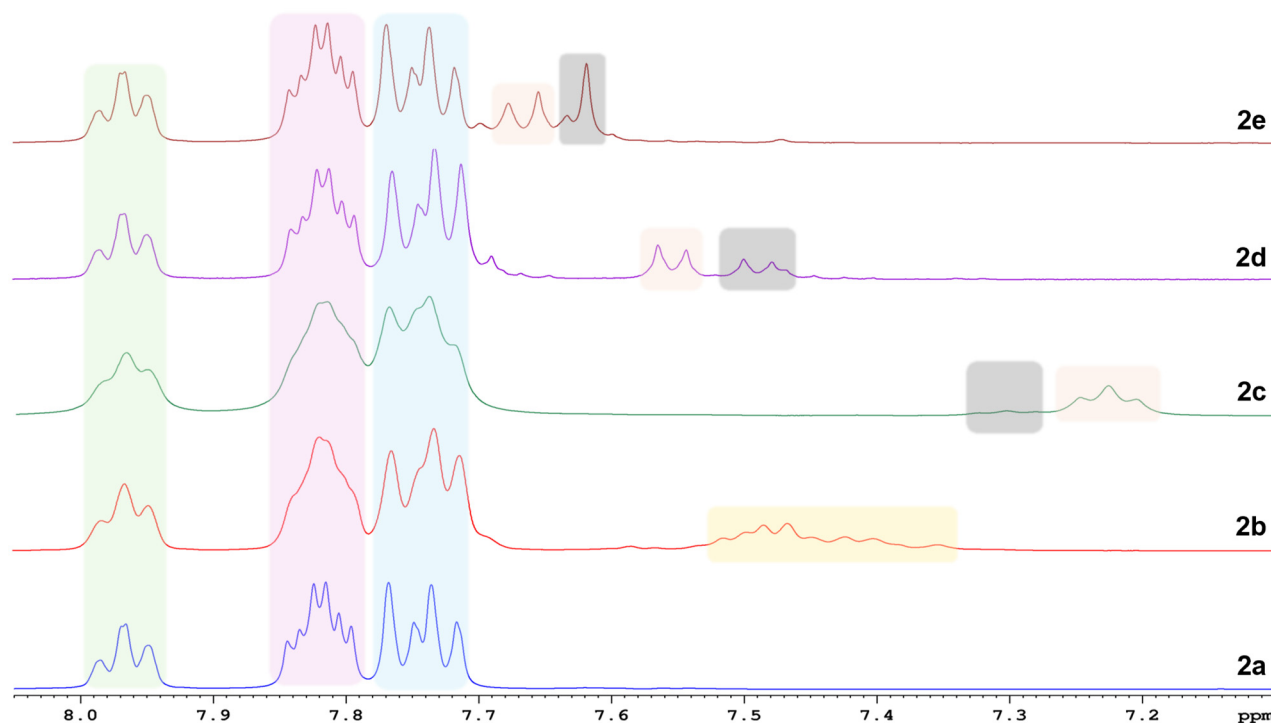


Fig. 3 ^1H -NMR spectra of **2a–e** stacked vertically in the 7.0 ppm to 8.0 ppm region. Ph_4P^+ -related ^1H peaks are grouped and color-coded, for which the light green region represents H_b , the light red region represents H_a/H_c , and the light blue region, H_d/H_e . Anion ^1H peaks are shown as light orange regions for H3/H5/H3'/H5' (**2c–e**) and as a light yellow region for H2/H2' to H6/H6' (**2b**). The light gray regions for each spectrum represent peaks possibly related to isomers.

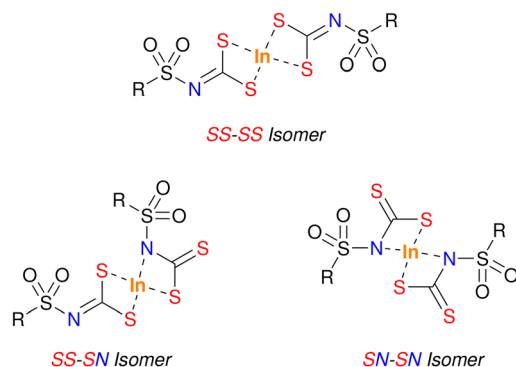


Fig. 4 Structural formulae for the constitutional isomers of **2a–f** according to the coordination mode. The SS–SS isomer involves the complexation of the dithiocarbamates by their sulfur atoms. The SS–SN isomer is formed by the complexation of one dithiocarbamate with its sulfur atoms and another dithiocarbamate with one sulfur atom and one nitrogen atom. Finally, the SN–SN isomer is formed by the dithiocarbamates with one sulfur atom and one nitrogen atom.

moiety would display the opposite pattern, furnishing a hypsochromic shift of the $\nu_{\text{as}} \text{CS}_2$ band compared to **1a–f**. The literature shows that $\nu_{\text{as}} \text{CS}_2$ in dithiocarbamate complexes, which have a formal $\text{C}=\text{S}$ bond, range from 990 cm^{-1} to 1100 cm^{-1} (ref. 39 and 40) and the FTIR spectra for **2a–f** showed one band at $998.40(57) \text{ cm}^{-1}$. Therefore, while the $951.2(16.6) \text{ cm}^{-1}$ band indicates an SS complexation, the one at $998.40(57) \text{ cm}^{-1}$ could indicate an SN complexation and serve as evidence of the formation of the specified isomers. However, the studies conducted by Adeyemi *et al.* and Halimehjani *et al.*,^{40,41} pertaining to the synthesis of *N*-substituted dithiocarbamate complexes, show $\nu \text{C–N}$ -related bands at $1231.63(3.81) \text{ cm}^{-1}$. Notably, the FTIR spectra of **2a–f** show no bands between 1265 cm^{-1} and 1139 cm^{-1} , indicating that SN-coordinated complexes are likely present as minor products and the SS–SS isomer is preponderant.

One interesting aspect of isomer formation was observed for **2e**, for which the ^{13}C -NMR spectra (Fig. S17†) showed two clear peaks at 200.4 ppm and 208.6 ppm. Choosing which peak would be correctly assigned to the $\text{C}=\text{N}$ carbon atom led to a systematic analysis of NMR spectroscopy data for all reported dithiocarbamate metal complexes, which ultimately led to assigning the 208.6 ppm peak to the $\text{C}=\text{N}$ carbon atom. This analysis considered 72 homoleptic sulfonyldithiocarbamate complexes spanning 27 publications^{25–27,35,42–64} and involved analyzing the correlation between the ^{13}C chemical shift of the $\text{C}=\text{N}$ carbon atom and (i) the charge of the complex, (ii) the metal, (iii) the outermost shell of the metal cation, (iv) the number of d electrons of the metal cation, (v) the counterion of the complex, (vi) the dithiocarbamate sulfonyl substituent, (v) the spectrometer frequency and (vi) the solvent used in spectra acquisition. First, a Spearman correlation matrix was constructed for these variables (Fig. 5), which indicated that the chemical shift correlated moderately with the charge of the complex (-0.60), the metal cation ($+0.5$), the number of d electrons of the metal cation (-0.56), the

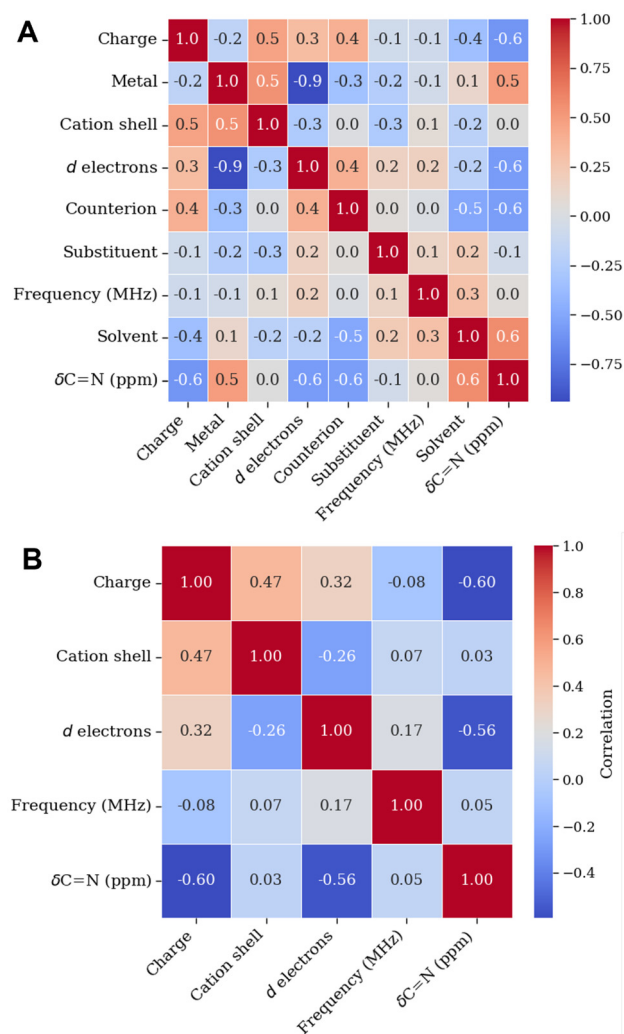


Fig. 5 Spearman correlation matrices for (A) all variables considered in the statistical analysis and for (B) the numerical variables—*i.e.*, complex charge, metal cation electron shell and d electron count of the metal cation in the complex, spectrometer frequency (MHz), and the ^{13}C chemical shift of the $\text{C}=\text{N}$ bond ($\delta \text{C}=\text{N}$ (ppm)).

counterion (-0.6), and the solvent ($+0.6$). It should be noted that the p -value for these correlations were all equal to 0.0, and that the Spearman correlation was favored over the Pearson's given the high condition number obtained by the OLS (Ordinary Least Squares) regression – *i.e.*, 2.17×10^3 .

Moreover, the variances of the chemical shift values ($\delta \text{C}=\text{N}$) across the charges of the complexes and the numbers of d electrons of the metal cations were analyzed by ANOVA (Analysis Of Variance). The analysis of the F -statistics values indicated a high variance of $\delta \text{C}=\text{N}$ between the groups compared to the variance among $\delta \text{C}=\text{N}$ values, and the p -values indicated that the groups are statistically different (Table 2). This indicated that they were the most impactful variables to the chemical shift, as shown in Fig. 6.

The d electron count for the metallic center reflects its electronic environment more accurately and was thusly chosen as

Table 2 *F*-Statistic and *p*-values for the ^{13}C chemical shift of the C=N carbon atom ($\delta \text{C}=\text{N}$ (ppm)), the complex charge, and the number of *d* electrons of the metal

Dependent variable	Categorical variable	<i>F</i> -Statistic	<i>p</i> -Value
$\delta \text{C}=\text{N}$ (ppm)	Complex charge	175.251	0.000
	<i>d</i> -Electron count	4.200	0.019

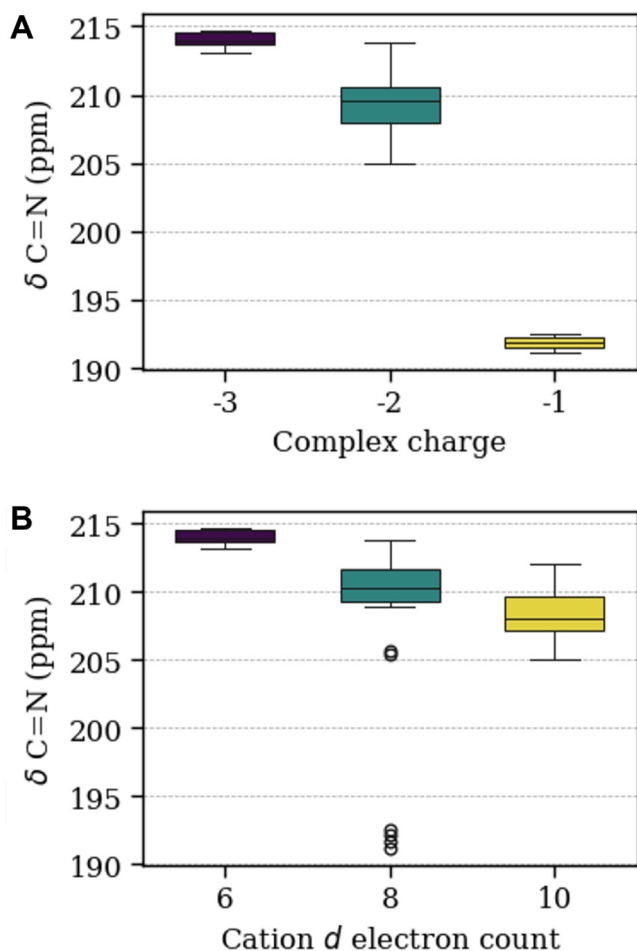


Fig. 6 Boxplots of ^{13}C chemical shifts of the C=N bond ($\delta \text{C}=\text{N}$ (ppm)) for homoleptic dithiocarbamate complexes in the literature. Panel A shows the variation of $\delta \text{C}=\text{N}$ according to the charge of the complex, and panel B shows their variation according to the number of *d* electrons of the cationic metal center.

the main categorical variable. One can see that a higher *d* electron count for the metal cation results in a greater shielding of the C=N carbon atom, which can be attributed to a possible metal–ligand backbonding for compounds **2a–f** that would be more pronounced in complexes with a higher *d* electron count at their metallic cation centers, increasing the electronic density at the NCS_2 group. The $\delta \text{C}=\text{N}$ values obtained in this work – *i.e.*, 207.5(2.81) ppm – agree with these findings, given that In(III) has 10 *d* electrons. The physical significance of the

inverse correlation between *d*-electron count and $\delta \text{C}=\text{N}$ was not immediately clear, and a significant lack of this kind of discussion was observed in the current dithiocarbamate literature. However, some initial theories could be formed based on findings for similar metallic complexes.

Gowda *et al.*⁶⁵ published an interesting study showing how DFT calculations can aid the assignment of solid-state NMR signals and provide a more accurate structure elucidation of a heteroleptic La(III) dithiocarbamate/phenanthroline complex. In this paper, the authors show that high Laplacian of the electron density ($\nabla\rho^2$) and negative energy density ($H(r)$) values for this complex point to a considerable covalent character for the La–S and La–N, with the latter being more covalent than the former. Moreover, a Natural Bond Orbital (NBO) analysis of the same complex revealed that the La–S bonding orbital is heavily polarized towards the sulfur atom (polarization coefficient = 0.96), and that all NBOs of the NCS_2 system are predominantly *p*-hybridized. These findings suggest that dithiocarbamates, which display the same chelate mode of coordination, could have an *S*-polarized In^{3+} –S bond, contributing to the shielding of the carbon atom of the NCS_2 moiety.

Additionally, Pd(II) (d^8) complexes with aromatic ligands were shown to display some degree of π back-bonding by Martinez-Vivente *et al.*,⁶⁶ demonstrating that this metal–ligand interaction promoted a shielding to the carbon atom at the *para* position to the Pd(II) center. Moreover, dithiocarbamates are strong σ -donor ligands which, coupled to the high *d*-electron count of In(III) , could promote a stronger π back-bonding, as observed for *N*-heterocyclic carbenes metallic complexes by Comas-Vives and Harvey.⁶⁷

Although the formation of the SS–SS, SS–SN, and SN–SN isomers could be inferred from the acquired data, the relative population of said isomers could not be attested from experimental data alone. At most, the data suggest that the size of the halogen bound to the aromatic ring is proportional to the amount of isomers present in the NMR sample, given the increasing complexity of the resulting spectra. Therefore, extensive computational calculations were performed to shed light on some thermodynamic aspects of these isomers. It should be noted that understanding the behavior of these isomers and, especially, knowing their relative stabilities is paramount to learning how they will behave biologically and what chemical transformations are adequate to modulate their activities.

In this sense, geometry optimization and frequency calculations were performed for compounds **2a–f** isomers using implicit solvation of water and DMSO to understand their relative stabilities. Table 3 gathers the Gibbs free energy difference results for the SN–SN and SN–SS isomers relative to their corresponding SS–SS isomer, once the SS–SS isomers were computed as the most stable among compounds **2a–f**. The SN–SS isomers have intermediate stability compared to the other two possibilities, and the SN–SN isomers were the least stable among **2a–f**. However, the energy difference does not follow the same pattern for the other two isomers. While the SN–SN molecules are *ca.* 8 kcal mol^{-1} higher in energy com-

Table 3 Gibbs free energy difference (in kcal mol^{−1}) relative to the corresponding SS–SS isomer using implicit solvation of DMSO and water and their corresponding equilibrium constant (K_{eq}) between SN–SS, SN–SN, and SS–SS isomers, and C=N chemical shifts (ppm, experimental and calculated) for compounds **2a–f**

Compound	Thermodynamic parameters ^a						Chemical shift ^b			
	DMSO			Water			Exp.	Calculated		
	ΔG_{SN-SN}	ΔG_{SN-SS}	K_{eq}	ΔG_{SN-SN}	ΔG_{SN-SS}	K_{eq}		SN–SN	SN–SS	SS–SS
2a	7.95	5.35	8355.6	7.95	5.32	7943.1	206.9	234.7(8)	221.4(13.5)	217.1(2)
2b	8.28	6.00	25 031.2	8.26	5.98	24 200.3	203.1	232.2(1)	221.8(13.5)	216.8(4)
2c	8.25	4.26	1327.1	8.36	4.17	1140.1	208.2	231.2(4)	223.4(11.3)	217.2(0)
2d	7.71	3.80	610.5	7.67	3.69	507.1	210.6	232.2(3)	224.0(10.1)	217.2(2)
2e	8.03	3.61	443.0	8.05	3.60	435.6	208.6	232.5(5)	224.0(9.9)	217.4(2)
2f	8.09	2.67	90.64	8.08	2.70	95.3	na ^c	232.3(0)	224.4(11.2)	217.4(2)

^a Calculations performed at B3LYP-D3(BJ)/def2-TZVP level of theory. ^b Calculations performed at B3LYP/def2-TVZPP level of theory. ^c The signal related to the C=N group for **2f** was not observed.

pared to the SS–SS, the relative stability of SN–SS molecules towards the same compounds varies significantly, showing a tendency of decreasing energy with increasing halogen size. While the energy difference between SN–SS and SS–SS isomers of **2c** is 4.26 kcal mol^{−1} and 4.17 kcal mol^{−1} in DMSO and water, respectively, the same comparison is 2.67 kcal mol^{−1} and 2.70 kcal mol^{−1} for **2f**, respectively. These results support the above findings, suggesting that more than one isomer is present, especially for compounds **2d–f**. In this sense, Table 3 also presents the equilibrium constant, K_{eq} , for the interconversion reaction assuming the SN–SS → SS–SS process in DMSO and water (implicit solvation), calculated using the vastly known $\Delta_r G^\circ = -RT \ln K_{eq}$ equation, where $\Delta_r G^\circ$ is the standard free Gibbs energy of reaction, R is the gas constant, and T is the temperature of 298.15 K. As can be observed, the solvent nature does not primarily affect the relative stability of the isomers, and the results in water and DMSO are very similar. For all compounds, $K_{eq} \gg 1$, which indicates that the reaction ultimately favors the formation of SS–SS isomers. Compounds **2e** and **2f** have the smallest K_{eq} , and the formation of the SN–SS isomers is possible, even if in small concentration. These results align with the observed experimental NMR results discussed previously.

Another crucial computational result on isomer formation was the calculated NMR chemical shifts of **2a–f** (Tables S2 and S3†). The compiled C=N chemical shift (δ) values (ppm) for each isomer of **2a–f** are shown in Table 3. The δ C=N was chosen due to its pronounced sensitivity to the coordination mode. Although the aromatic protons H3/H5/H3'/H5' of **2c–f** yielded pronounced neighboring, low-intensity signals, as previously discussed (Fig. 3), their calculated NMR δ were not sufficiently different to provide meaningful results pertaining isomer prevalence. Notably, the non-zero standard deviation of the δ C=N for the isomers and its high value for the SN–SS – ca. 11.2 – is due to a non-equivalence of the carbon atoms for each sulfonyldithiocarbamate ligand in the complex. This non-equivalence, while minimal for the SN–SN and SS–SS isomers, is substantial for the SN–SS isomer. Specifically, the calculated δ C=N is 231.4(5) ppm for the SN-coordinated ligand and

215.0(2.3) ppm for SS-coordinated ligand. Nevertheless, the calculated data reveal that the SS-coordinated ligands have significantly more shielded C=N carbons than the SN-coordinated ones. Moreover, the experimental shifts are closer to the calculated ones for the SS–SS isomers, corroborating its preponderance in lieu of the other two. Considering that the NMR spectra showed no evidence of two C=N-related signals after a single analysis, the prevalence of the SN–SS can also be considered minimal.

The relative stability of the isomers was also investigated by analyzing the highest occupied molecular orbital, HOMO, of each compound. Fig. 7 shows the HOMO of all three isomers of compounds **2c** and **2f**, which feature fluorine and iodine atoms, respectively. The delocalization of the electron density is more pronounced in the SS–SS isomer for both compounds when compared with the other two isomers. Furthermore, the iodine atom has a bigger orbital coefficient contributing more to the HOMO in the SS–SS isomer case. The HOMO of **2a–b** and **2d–e** compounds are shown in the ESI (Fig. S20†).

2.2. Biological assays

Table 4 presents the IC₅₀ (μmol L^{−1}) values of compounds **2a–f** in human tumor (HCT-116, SK-MEL-28, and MCF-7) and non-tumor (HaCaT) cell lines.

Compounds **2a–f** exhibited varying levels of cytotoxicity depending on the cell line treated (Fig. S21–S26†). Overall, HCT-116 cells were the most sensitive, with IC₅₀ values below 5.5 μmol L^{−1} for all tested compounds. **2a** demonstrated the highest cytotoxicity against HCT-116, with an IC₅₀ of 3.02(21) μmol L^{−1}, whereas **2f** was the least cytotoxic, with an IC₅₀ of 5.36(42) μmol L^{−1}. In contrast, SK-MEL-28 and MCF-7 cells exhibited poor cytotoxicity, with IC₅₀ values often exceeding 30 μmol L^{−1}.

Regarding the human keratinocyte cell line (HaCaT), compounds **2a–f** induced low toxicity to non-tumor cells, which was suggested by their IC₅₀ values above 100 μmol L^{−1}. Doxorubicin (DXR), used as a positive control, exhibited high cytotoxicity against all tumor (HCT-116 IC₅₀ = 2.570(1) μmol L^{−1}; SKMEL-28 IC₅₀ = 3.55(1.67) μmol L^{−1}; MCF-7 IC₅₀ = 1.53

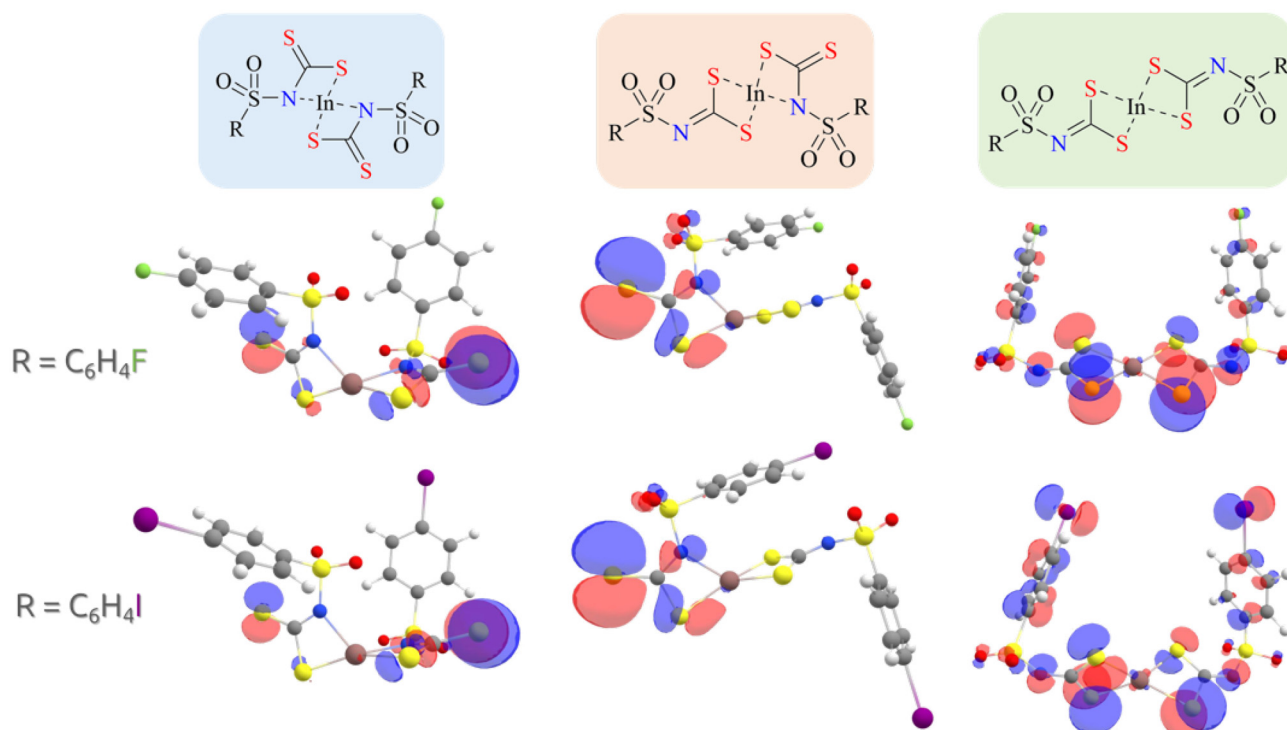


Fig. 7 The highest occupied molecular orbitals, HOMO, of SN-SN, SN-SS, and SS-SS isomers in DMSO of compounds **2c** and **2f**.

Table 4 Cytotoxic activity (IC_{50} , $\mu\text{mol L}^{-1}$) of compounds **2a–f** and doxorubicin (DXR) against human tumor – *i.e.*, HCT-116 (colorectal adenocarcinoma), SK-MEL-28 (melanoma), MCF-7 (breast adenocarcinoma) –, and non-tumor – *i.e.*, HaCaT (keratinocytes) – cell lines after 72 hours of treatment. Doxorubicin (DXR) was used as the positive control

Compound	IC_{50} ^a ($\mu\text{mol L}^{-1}$)			
	HCT-116	SK-MEL-28	MCF-7	HaCaT
2a	3.02(21)	38.29(3.21)	34.70(2.31)	>100
2b	3.58(29)	43.30(4.15)	89.90(14.7)	>100
2c	5.19(60)	45.68(3.26)	47.35(4.48)	>100
2d	4.14(24)	40.22(3.45)	96.33(12.3)	>100
2e	3.15(1.42)	54.31(5.52)	32.26(3.23)	>100
2f	5.36(42)	37.53(3.04)	77.10(11.5)	>100
DXR	2.570(1)	3.55(1.67)	1.53(20)	0.280(1)

^a Values were obtained by nonlinear regression from at least three independent experiments performed in quadruplicate and are expressed as mean(SEM) – *i.e.*, $\bar{x}(\text{SEM})$.

(20 $\mu\text{mol L}^{-1}$) and non-tumor cells (HaCaT IC_{50} = 0.280(1) $\mu\text{mol L}^{-1}$), suggesting a lack of selectivity. In contrast, compounds **2a–f** demonstrated preferential cytotoxicity against tumor cells, indicating a degree of tumor selectivity, a desirable feature that could reduce adverse effects in clinical applications.⁹

Analyzing the cytotoxicities of compounds **2a–f** against human colorectal adenocarcinoma cell lines – *i.e.*, HCT-116 – (Fig. 8) revealed a non-linear relationship between the dithiocarbamate substituents and the biological activity. While the

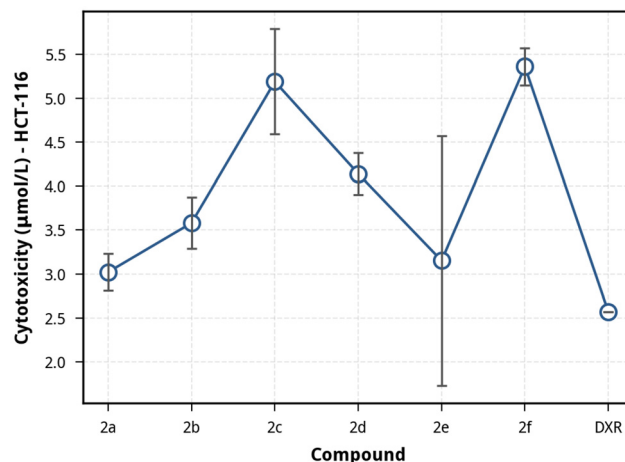


Fig. 8 Cytotoxicity values (IC_{50} , $\mu\text{mol L}^{-1}$) of compounds **2a–f** against HCT-116 (colorectal adenocarcinoma) cell lines after 72 hours of treatment with the respective error bars. Doxorubicin (DXR) was used as the positive control.

methyl and 4-bromophenyl substituents – **2a** and **2e**, respectively – were responsible for the most active complexes, with IC_{50} values comparable to DXR, clear trends could not be established. On the one hand, changing the *para* aromatic substituent from fluorine (**2c**) to chlorine (**2d**) to bromine (**2e**) yielded increasing cytotoxicities. However, this trend is interrupted by the inferior activity of **2f**, with its 4-iodophenyl group. Interestingly, the least active complexes against

HCT-116 – viz., **2c** and **2f** – showed the smallest cytotoxicities against HaCaT cell lines, alluding to a higher selectivity, and the aliphatic In(III) dithiocarbamate complex **2a** was more active than its aromatic counterparts **2b–f**.

Although some aspects of the antineoplastic activities of **2a–f** need further experiments to be adequately explained, some studies can provide indications of their mechanism of action. Traditionally, metal dithiocarbamate complexes are tested as antimicrobial crop-preserving agents. For instance, Zn(II) dithiocarbamate complexes were investigated by Rabello *et al.* as control agents for coffee leaf rust, caused by *Hemileia vastarix* (Puccinialis), and aliphatic dithiocarbamates showed greater antifungal capabilities than aromatic ones.⁶⁸ However, halogen-related trends were not compatible with the one observed herein. Alternatively, Sn(IV) complexes of the form R_2SnL_2 , where L is an aromatic dithiocarbamate, were evaluated by Dias *et al.* as inhibitors of *Colletotrichum gloeosporioides*, which did not show a clear trend for the aromatic substituents.⁶⁹ Therefore, it is clear that the previous results of the antimicrobial activity cannot be used as a reference point for the present discussion, likely due to a markedly different mechanism of action.

Fortunately, Castro *et al.* published a recent study about the antitumor activities of two potassium Pt(II) sulfonyldithiocarbamate complexes – i.e., $K_2 [Pt(CH_3SO_2N=CS_2)_2]$ and $K_2 [Pt(4-FC_6H_5SO_2N=CS_2)_2]$.¹⁶ The interactions between these compounds with biotin-labeled λ -DNA revealed that the aliphatic dithiocarbamate complex performs minor groove binding.^{70,71} In contrast, the aromatic dithiocarbamate complex performs intercalation at $<30 \mu\text{mol L}^{-1}$, and aggregate-induced groove binding at $>30 \mu\text{mol L}^{-1}$. A similar DNA intercalation behavior was observed for a Pd(II) dithiocarbamate/phenanthroline complex by Feizi-Dehneyebi *et al.*⁷²

Another critical study in this field was published by Adeyemi *et al.*, which analyzed the cytotoxicities against the human tumor cell line (HeLa) of Sn(IV) dithiocarbamate complexes of the form R_2SnL_2 , where L is an *N,N*-diallyldithiocarbamate and $R = \text{Cl}, \text{CH}_3, \text{C}_4\text{H}_9$, and C_6H_5 .⁷³ The researchers noticed that the cytotoxicity of the complex was intrinsically related to its lipophilicity – e.g., the observed IC_{50} values for $[\text{Ph}_2\text{SnL}_2]$, $[(\text{CH}_3)_2\text{SnL}_2]$, and $[(\text{C}_4\text{H}_9)_2\text{SnL}_2]$ were $2 \mu\text{mol L}^{-1}$, $56 \mu\text{mol L}^{-1}$, and $288 \mu\text{mol L}^{-1}$, respectively.

A common ground capable of reconciling these findings with the observed cytotoxicities of **2a–f** can be related to the interplay between (i) the degree of halogen bonds of **2c–f** and the DNA base pairs of the tumor cell lines, (ii) the steric hindrance associated with intercalation or groove binding, and (iii) the lipophilicity of the dithiocarbamate portion of **2a–f**. Halogen bonds⁷⁴ have been associated with cytotoxicities, as observed by Kitawat and Singh in the investigation of the DNA binding properties of halogenated chalcones, which showed a stronger binding for the brominated compound compared to the chlorinated and fluorinated analogs.⁷⁵ Notwithstanding, Arjmand *et al.* observed that halogenated Cu(II) chromone complexes display DNA intercalation with intrinsic binding constants, K_b , proportional to halogen size given the increase in halogen bond strength.⁷⁶

The activity of the metallic complexes **2a–f** could not be compared to their potassium dithiocarbamate precursors **1a–f**. This is due to the unavoidable decomposition of dithiocarbamates when left in aqueous or organic solutions for a long time and was experimentally observed in some instances by our group – characterized by the evolution of a sulfur-like smell and a color shift to white. However, our group managed to isolate a white single crystal of the decomposition product and analyze it by X-ray crystal diffraction. To our knowledge, this is the first report on the structural analysis of potassium dithiocarbamate decomposition products. However, it should be noted that decomposition of the potassium dithiocarbamates during the reaction to form **2a–f** is highly unlikely given the speed of complexation, which is almost immediately observed by the disappearance of the characteristic yellow hue associated with **1a–f**.

Finally, the cell viability-concentration profiles of **2a–f** (Fig. S21–S26†) show that, for the tumor cell lines MCF-7, SK-MEL-28, and HCT-116, the cell viability tends to decrease to its lowest value after a specific concentration, displaying a plateau-like behavior for higher concentrations. Conversely, analyses using the non-tumor cell line HaCaT showed that all compounds except **2c** and **2f** have a sudden drop in cell viability at $200 \mu\text{mol L}^{-1}$. This prompted a deeper analysis of the cytotoxic behavior of **2a–f**.

Analyzing the cell viability-concentration profiles of DXR against these cell lines (Fig. S27†) reveals a similar profile, lowering the likelihood of a compound-specific behavior. Moreover, the stability of the In(III) complex **2a**, which displayed the most pronounced activity, was analyzed in phosphate-buffered saline (PBS) with DMSO (0.5%) and pH 7.4 by UV-Vis spectroscopy (Fig. 9). The results indicate that **2a** is stable in these conditions, given that the spectral profile did not change for 72 hours. Therefore, **2a** retains its chemical and structural integrity throughout the biological assay, and no degradation products were formed during this time.

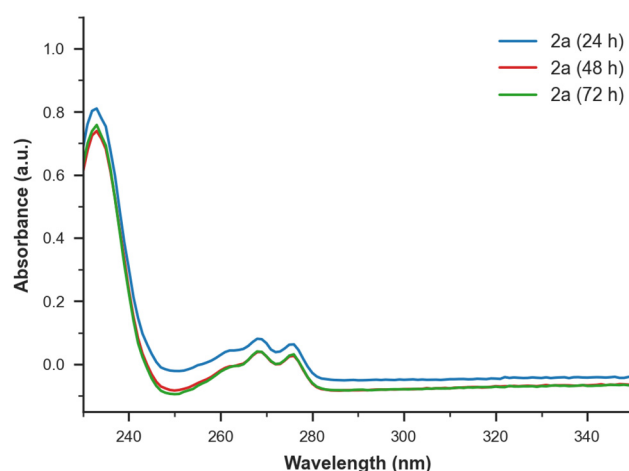


Fig. 9 UV-Vis absorption spectra obtained from the stability analysis of compound **2a** in PBS with DMSO (0.5%), pH 7.4, after 24 h, 48 h, and 72 h in solution.

Hence, possible alternative reasons underlying the displayed cell viability-concentration profiles for **2a–f** include the saturation of intracellular molecular targets or cellular uptake mechanisms. Once a concentration sufficient to engage the primary cytotoxic mechanism – *e.g.*, DNA interaction, redox imbalance, or mitochondrial dysfunction – is reached, increasing the dose may not enhance the effect due to target saturation or limited uptake. Additionally, the initial response might reflect a predominantly cytostatic effect, such as cell cycle arrest or senescence, rather than direct cell death. In this case, metabolic activity measured by the MTT assay may reach a plateau as proliferation and mitochondrial function decrease, even though the cells remain viable but metabolically inactive. This phenomenon has been described for other metal-based compounds and may contribute to the flattened curve at higher concentrations.⁷⁷

2.3. Crystal data

Crystal data and selected geometrical parameters of the decomposition product of **1b** are listed in Table 5 and in the ESI (Table S4†), respectively. The crystal fragment of the decomposition product is displayed in Fig. 10A. The final compound is a bi-dimensional coordination polymer formed by K–S and K–O coordination bonds. The potassium cation is coordinated to seven atoms – five oxygen atoms and two sulfur atoms –, giving rise to a capped trigonal prismatic geometry. The average K–O bond distance is 2.382(2) Å and, for K–S, is 3.2349(8) Å. The torsion angle between the aromatic ring and the SO₂–N–CSO–C group is 79.5°. The solid state is stabilized by K–O and K–S coordination and C–H... π interactions (distance H...centroid = 3.32 Å and 3.42 Å). The topological analysis⁷⁸ of **1b** indicates that the bidimensional net is unimodal,

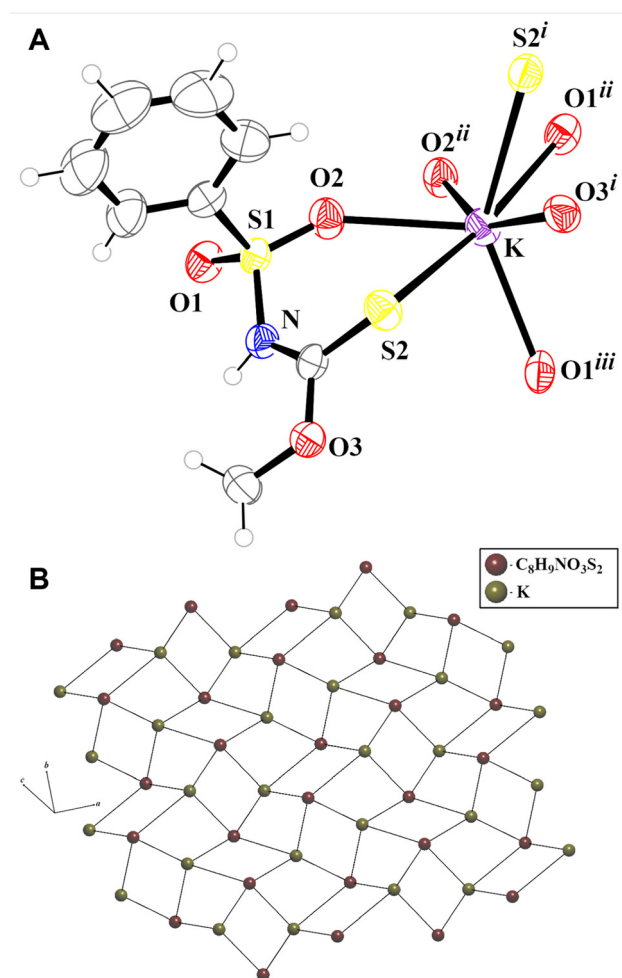


Fig. 10 (A) Fragment of the crystal structure of compound **1b**, showing thermal ellipsoids at 50% probability level, and (B) simplified *sql* net. Symmetry code: i: $\frac{1}{2} - x, \frac{1}{2} + y, z$, ii: $1 - x, 2 - y, 1 - z$, iii: $x - \frac{1}{2}, 1.5 - y, 1 - z$, iv: $\frac{1}{2} - x, y - \frac{1}{2}, z$.

Table 5 Crystal data and structure refinement results for the crystal of compound **1b**

Compound	1b
Molecular formula	C ₈ H ₉ NO ₃ S ₂ K
Molar mass/g mol ^{−1}	270.38
Crystal system	Orthorhombic
Space group	<i>Pbca</i>
Crystal color	White
<i>a</i> /Å	11.1836(1)
<i>b</i> /Å	8.8869(1)
<i>c</i> /Å	23.2030(2)
α, β, γ /°	90.00, 90.00, 90.00
<i>V</i> /Å ³	2306.09(4)
Temperature/K	301(2)
<i>Z</i>	8
<i>D</i> _{calc} /g cm ^{−3}	1.558
Crystal size/mm	0.06 × 0.12 × 0.29
μ (Mo–K α)/cm ^{−1}	7.337
Measured/unique reflections	49 673/2520
<i>R</i> _{int}	0.0913
Observed reflections [<i>F</i> _o ² > 2 σ (<i>F</i> _o ²)]	2388
Refined parameters	137
<i>R</i> _{obs} [<i>F</i> _o > 2 σ (<i>F</i> _o)]/ <i>R</i> _{all}	0.0398/0.0412
<i>wR</i> _{obs} [<i>F</i> _o ² > 2 σ (<i>F</i> _o ²)]/ <i>wR</i> _{all}	0.1101/0.1114
<i>S</i>	1.061
RMS/e Å ^{−3}	0.076

tetra-connected, and it can be classified as *sql* type⁷⁹ with symbol point 4⁴·6². The simplified net *sql* is displayed in Fig. 10B. Notably, the decomposition of **1b** yielded a supramolecular-like network, which justifies the insolubility of the decomposition product in water.

3. Experimental section

3.1. Chemistry

All chemical compounds used in the syntheses and the deuterated reagents used for NMR analyses were purchased from Sigma-Aldrich (USA). The reagents were used without further purification. The solvents employed in the syntheses were purchased from Vetec Química Fina (Brazil).

¹H-NMR and ¹³C-NMR were recorded on a Bruker Avance III Nanobay spectrometer (400 MHz) at the Laboratório de Ressonância Magnética de Alta Resolução – LAREMAR – at the Federal University of Minas Gerais (UFMG), using DMSO-*d*₆ as

solvent and tetramethylsilane (TMS) as the internal standard. NMR spectra were also recorded on a Varian Mercury-300 spectrometer at the Chemistry Department of the Federal University of Viçosa (UFV). Correlation experiments were performed for the structural characterization of the products. IR spectra were recorded on a Spectrum 100 (PerkinElmer) scanning from 4000 cm^{-1} to 650 cm^{-1} . Mass spectra were recorded on a Bruker Daltonics model 9.4 T Solarix ultra-high resolution mass spectrometer operated in the negative and positive ionization modes over a mass range of m/z 200–2000 using Electron Spray Ionization Fourier Transform Ion Cyclotron Resonance Mass Spectrometry (ESI-FT-ICR MS). ESI-FT-ICR MS spectra were acquired with a resolving power of $m/\Delta m_{50\%} \sim 500\,000$, in which $\Delta m_{50\%}$ is the full peak width at the half-maximum peak height of m/z 400 and mass accuracy of <1 ppm, which provides an unambiguous molecular formula. The acquired spectra are shown in the ESI (Fig. S2†).

3.2. Chemical synthesis

The potassium *N*-R-sulfonyldithiocarbamate dihydrated salts, with the general formula $\text{K}_2(\text{R}-\text{SO}_2=\text{CS}_2) \cdot 2\text{H}_2\text{O}$, where $\text{R} = \text{CH}_3$ (**1a**), C_6H_5 (**1b**), $4\text{-FC}_6\text{H}_4$ (**1c**), $4\text{-ClC}_6\text{H}_4$ (**1d**), $4\text{-BrC}_6\text{H}_4$ (**1e**), and $4\text{-IC}_6\text{H}_4$ (**1f**) were prepared from the sulfonamides as described in the literature (Fig. 1).^{17–19} The complete procedure used to synthesize **1a–f** is described in the ESI.†

The syntheses of compounds **2a–f** (Fig. 1) were performed by adding 2 mmol of the appropriate dithiocarbamate salt (**1a–f**) to a 50 mL round-bottom flask, and dissolving the reagent in 20 mL of a methanol:water 1:1 (v:v) solution. 1 mmol (0.3008 g) of In(III) nitrate ($\text{In}(\text{NO}_3)_3$) was then added, resulting in the disappearance of the yellow color of the solution, and it was stirred for five minutes. 1 mmol (0.3749 g) of tetraphenylphosphonium chloride (PPh_4Cl) was dissolved in 500 μL of distilled water and added dropwise to the round-bottom flask, furnishing a white precipitate. The resulting solid was then filtered through a glass funnel with a sintered disc (G4) and washed with significant amounts of water, drops of ethanol, and small amounts of cold diethyl ether, yielding In(III) complexes **2a–f** as white solids with 38% to 98% yield.

The NMR spectra for compounds **2a–f** (Fig. 11) showed the expected signals for the tetraphenylphosphonium cation (Ph_4P^+) at: $^1\text{H-NMR}$ (400 MHz, DMSO-d_6) δ : 7.71–7.78 (m, 8H, Hb/Hf), 7.79–7.86 (m, 8H, Hc/He), 7.95–8.00 (m, 4H, Hd); and

$^{13}\text{C-NMR}$ (100 MHz, DMSO-d_6) δ : 118.2 (Ca, d, $^1J_{\text{C-P}} = 89$ Hz), 131.0 (Cb/Cf, d, $^2J_{\text{C-P}} = 13$ Hz), 135.0 (Cc/Ce, d, $^3J_{\text{C-P}} = 11.0$ Hz), 135.8 (Cd, d, $^4J_{\text{C-P}} = 3.0$ Hz).

3.2.1. Tetraphenylphosphonium bis(*N*-(methylsulfonyl)dithiocarbamate)In(III) (2a**).** White solid; yield = 75%; IR (ATR, cm^{-1}) 3169, 3078, 3056, 3033, 1585, 1483, 1435 (ν C=N), 1359, 1307, 1267, 1105, 995 (ν_{as} CS_2 , SN-SS/SN-SS), 944 (ν_{as} CS_2 , SS-SS), 924, 829, 753, 720, 687; $^1\text{H-NMR}$ (In(III) complex signals, 400 MHz, DMSO-d_6) δ : 2.83 (s, 6H, CH_3); $^{13}\text{C-NMR}$ (In(III) complex signals, 100 MHz, DMSO-d_6) δ : 38.9 (CH_3), 206.9 (C=N); HRMS (ESI) m/z calculated for $\text{C}_4\text{H}_6\text{InN}_2\text{O}_4\text{S}_6^-$ 452.76961, found 452.76959 (r.e. = 0.04 ppm).

3.2.2. Tetraphenylphosphonium bis(*N*-(phenylsulfonyl)dithiocarbamate)In(III) (2b**).** White solid; yield = 98%; IR (ATR, cm^{-1}) 3059, 1586, 1436 (ν C=N), 1376, 1280, 1141, 1083, 996 (ν_{as} CS_2 , SN-SS/SN-SS), 938 (ν_{as} CS_2 , SS-SS), 824, 719, 686; $^1\text{H-NMR}$ (In(III) complex signals, 400 MHz, DMSO-d_6) δ : 7.35–7.59 (m, 10H, H-2 to H-6, H-2' to H-6'); $^{13}\text{C-NMR}$ (In(III) complex signals, 100 MHz, DMSO-d_6) δ : 127.8 (C2/C6, C2'/C6'), 128.6 (C3/C5, C3'/C5'), 131.8 (C4, C4'), 203.1 (C=N); HRMS (ESI) m/z calculated for $\text{C}_{14}\text{H}_{10}\text{InN}_2\text{O}_4\text{S}_6^-$ 576.80091, found 576.80057 (r.e. = 0.59 ppm).

3.2.3. Tetraphenylphosphonium bis(*N*-(4-fluorophenylsulfonyl)dithiocarbamate)In(III) (2c**).** White solid; yield = 57%; IR (ATR, cm^{-1}) 3060, 1588, 1491 (ν C=N), 1372, 1280, 1140, 1082 (ν_{as} CS_2 , SN-SS/SN-SS), 938 (ν_{as} CS_2 , SS-SS), 834, 721, 687; $^1\text{H-NMR}$ (In(III) complex signals, 400 MHz, DMSO-d_6) δ : 7.23 (t, 4H, $^3J_{\text{H-F-H}} = 8.3$ Hz, H3/H5, H3'/H5'), 7.97 (t, 4H, $^4J_{\text{H-F-H}} = 6.7$ Hz, H2/H6, H2'/H6'); $^{13}\text{C-NMR}$ (In(III) complex signals, 100 MHz, DMSO-d_6) δ : 115.3 (d, $^2J_{\text{C-F}} = 22$ Hz, C3/C5, C3'/C5'), 130.6 (d, $^3J_{\text{C-F}} = 9$ Hz, C2/C6, C2'/C6'), 140.2 (d, $^4J_{\text{C-F}} = 3.0$ Hz, C1, C1'), 163.7 (d, $^1J_{\text{C-F}} = 247$ Hz, C4, C4'), 208.2 (C=N); HRMS (ESI) m/z calculated for $\text{C}_{14}\text{H}_8\text{F}_2\text{InN}_2\text{O}_4\text{S}_6^-$ 612.78107, found 612.78283 (r.e. = 1.24 ppm).

3.2.4. Tetraphenylphosphonium bis(*N*-(4-chlorophenylsulfonyl)dithiocarbamate)In(III) (2d**).** White solid; yield = 66%; IR (ATR, cm^{-1}) 3059, 1584, 1475 (ν C=N), 1367, 1272, 1141, 1082 (ν_{as} CS_2 , SN-SS/SN-SS), 938 (ν_{as} CS_2 , SS-SS), 818, 720; $^1\text{H-NMR}$ (In(III) complex signals, 400 MHz, DMSO-d_6) δ : 7.55 (d, 4H, $^3J_{\text{H-H}} = 8.5$ Hz, H3/H5, H3'/H5'), 7.79–7.84 (m, 4H, H2/H6, H2'/H6'); $^{13}\text{C-NMR}$ (In(III) complex signals, 100 MHz, DMSO-d_6) δ : 128.8 (C2/C6, C2'/C6'), 129.8 (C3/C5, C3'/C5'), 141.4 (C1, C1'), 210.7 (C=N); HRMS (ESI) m/z calculated for $\text{C}_{14}\text{H}_8\text{Cl}_2\text{InN}_2\text{O}_4\text{S}_6^-$ 644.72296, found 644.72273 (r.e. = 0.36 ppm).

3.2.5. Tetraphenylphosphonium bis(*N*-(4-bromophenylsulfonyl)dithiocarbamate)In(III) (2e**).** White solid; yield = 73%; IR (ATR, cm^{-1}) 3058, 1573, 1483, 1436 (ν C=N), 1367, 1270, 1139, 1072 (ν_{as} CS_2 , SN-SS/SN-SS), 938 (ν_{as} CS_2 , SS-SS), 815, 720, 686; $^1\text{H-NMR}$ (In(III) complex signals, 400 MHz, DMSO-d_6) δ : 7.67 (d, 4H, $^3J_{\text{H-H}} = 9.0$ Hz, H3/H5, H3'/H5'), 7.79–7.84 (m, 4H, H2/H6, H2'/H6'); $^{13}\text{C-NMR}$ (In(III) complex signals, 100 MHz, DMSO-d_6) δ : 125.5 (C4, C4'), 131.4 (C3/C5, C3'/C5'), 131.7 (C2/C6, C2'/C6'), 143.1 (C1, C1'), 208.6 (C=N); HRMS (ESI) m/z calculated for $\text{C}_{14}\text{H}_8\text{Br}_2\text{InN}_2\text{O}_4\text{S}_6^-$ 734.61989, found 734.61919 (r.e. = 0.95 ppm).

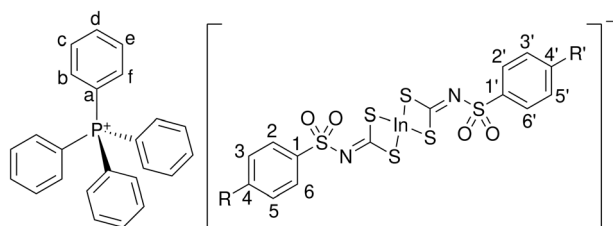


Fig. 11 General structure and atom numbering of tetraphenylphosphonium In(III) sulfonyldithiocarbamate salts (**2a–f**).

3.2.6. Tetraphenylphosphonium bis(*N*-(4-iodophenylsulfonyl)dithiocarbamate)In(III) (2f). White solid; yield = 38%; IR (ATR, cm⁻¹) 3057, 1568, 1436 (ν C=N), 1380, 1288, 1142, 1080 (ν_{as} CS₂, SN-SS/SN-SN), 933 (ν_{as} CS₂, SS-SS), 812, 721; ¹H-NMR (In(III) complex signals, 400 MHz, DMSO-d₆) δ : 7.49 (d, 4H, ³J_{H-H} = 6.92 Hz, H3/H5, H3'/H5'), 7.82–7.87 (m, 4H, H2/H6, H2'/H6'); ¹³C-NMR (In(III) complex signals, 100 MHz, DMSO-d₆) δ : 129.8 (C3/C5, C3'/C5'), 130.8 (C2/C6, C2'/C6'), 137.3 (C4, C4'), 137.5 (C1, C1'); HRMS (ESI) *m/z* calculated for C₁₄H₈I₂InN₂O₄S₆⁻ 828.59419, found 824.59418 (r.e. = 0.01 ppm).

3.3. Computational details

All calculations in this work were performed employing ORCA-5.0.4 software.^{80,81} Full unconstrained geometry optimizations and frequency calculations were carried out for the three possible isomers of molecules **2a–f** to determine the relative stability of the SN-SN, SN-SS, and SS-SS. A scaling factor of 0.97 was applied to the frequencies of the normal modes calculated.^{82–84} Density Functional Theory (DFT) was used with the hybrid functional B3LYP.⁸⁵ The Ahlrichs def2-SVP basis set^{86,87} was used for the optimizations and frequencies, while the def2-TZVP basis set^{86,87} was used for single-point calculations. All calculations included the Grimme's D3 dispersion correction⁸⁸ with Becke–Johnson (BJ) damping.⁸⁹ Coulomb integrals were sped up by RICOSX approximation⁹⁰ using def2/J as an auxiliary basis set.⁹¹ The conductor-like polarizable continuum model (C-PCM)⁹² was used to simulate implicit solvation in water and DMSO. Mayer bond order of the molecules **2a–f** was also evaluated.

From the optimized geometries of the isomers, NMR chemical shift calculations were performed with B3LYP/def2-TZVPP^{85–87} level of theory and C-PCM⁹² to simulate DMSO solvation. Tetramethylsilane (TMS) was chosen as the reference molecule, and all calculated chemical shifts presented herein are given as the TMS average chemical shift absolute value minus the chemical shift absolute value of each carbon or hydrogen atom of the isomers.

3.4. Single crystal X-ray diffraction

A Sinergy diffractometer was used to collect the measures for the crystallographic determination, with copper radiation (λ = 1.54184 Å) at ambient temperature. The data collection and reduction were processed in the CrysAlisPro software.⁹³ OLEX2⁹⁴ was employed in conjunction with the SHELXL suite of crystallographic programs⁹⁵ for structure resolution and refinement. Non-hydrogen atoms were refined with anisotropic thermal parameters. C- and N-bonded H atoms were placed in idealized positions and treated by a rigid model, with $U_{iso}(H)$ = 1.2 $U_{eq}(C/N)$ for aromatic and NH groups, and $U_{iso}(H)$ = 1.5 $U_{eq}(C)$ for methyl groups. The figures were made in ORTEP-3 for Windows⁹⁶ and ToposPro.⁹⁷ The crystallographic information file (CIF) containing complete data on the structural studies has been deposited in the Cambridge Crystallographic Data Center (CCDC) database under number 2433188.†

3.5. Biological assays

3.5.1. Cell lines. The MCF-7 (breast adenocarcinoma), SK-MEL-28 (human melanoma), HCT-116 (colorectal adenocarcinoma), and HaCat (human immortalized keratinocytes) cell lines were obtained from Rio de Janeiro Cell Bank (BCRJ, Rio de Janeiro, Brazil), and cultured in Dulbecco's modified Eagle's medium (DMEM) (MCF-7, SK-MEL-28 and HaCaT) or Roswell Park Memorial Institute 1640 (RPMI) (HCT-116) medium supplemented with 10% Fetal Bovine Serum and 1% penicillin–streptomycin, at 37 °C, with 5% CO₂.

3.5.2. Cytotoxicity assay against tumor and non-tumor cells. The MTT assay (3-(4,5-dimethylthiazol-2-yl)-2,5-diphenyltetrazolium bromide) was used to evaluate the cytotoxicity of indium compounds against MCF-7 (breast adenocarcinoma), SK-MEL-28 (human melanoma), and HCT-116 (colorectal adenocarcinoma) cell lines, as well as the non-tumor cells HaCaT (human immortalized keratinocytes). This method assesses cell viability and proliferation based on the reduced activity of mitochondrial and cytoplasmic enzymes. MTT, a water-soluble yellow dye, is converted into insoluble blue-purple formazan crystals within the cytosol of viable cells by the activity of dehydrogenases, primarily succinate dehydrogenase, which cleave the tetrazolium ring. The crystals are released and solubilized following cell lysis, enabling quantification *via* spectrophotometry.^{98,99}

The solid complexes were initially dissolved in DMSO to prepare stock solutions (20 mmol L⁻¹), which were then diluted in the culture medium immediately prior to treatment. The final DMSO concentration in all assays was maintained at or below 0.5% (v:v). Cells (100 μ L per well) were seeded in 96-well plates at densities of 1×10^5 cells per mL (MCF-7) and 3×10^5 cells per mL (SKMEL-28, HCT-116, HaCaT). After 24 hours, the cells were treated with **2a–f** (100 μ L) at various concentrations (0.39 μ mol L⁻¹, 0.78 μ mol L⁻¹, 1.56 μ mol L⁻¹, 6.25 μ mol L⁻¹, 12.5 μ mol L⁻¹, 25 μ mol L⁻¹, 50 μ mol L⁻¹, 100 μ mol L⁻¹, and 200 μ mol L⁻¹), for 72 hours. Doxorubicin (DXR) was used as the standard for comparison. Following treatment, 110 μ L of supernatant was removed, and 10 μ L of a 5 mg mL⁻¹ MTT solution (Sigma-Aldrich, St Louis, MO, USA) was added to each well. Plates were incubated for an additional 4 hours, after which 100 μ L of a 10% (m:v) sodium dodecyl sulfate (SDS) solution was added to dissolve the formazan crystals.^{100,101} Absorbance was measured using a spectrophotometer (BioTek Instruments microplate reader, Synergy HT, Winooski, VT, USA) at a wavelength of 570 nm and used to calculate the IC₅₀ (half-maximal inhibitory concentration). Three independent experiments were performed in quadruplicate.

3.5.3. Statistical analyses. Statistical analysis was performed using GraphPad Prism 8.0.2 (Graphpad Software Inc., San Diego, CA, USA). Results are expressed as the mean (standard deviation) – *i.e.*, $\bar{x}(\sigma)$. Data statistical analysis was performed using Analysis of Variance (ANOVA), followed by Tukey's test ($p < 0.05$). The half-maximal inhibitory concentrations (IC₅₀) and their 95% confidence intervals (CI 95%) were obtained by non-linear regression analysis.

3.5.4. Stability analysis of **2a** using UV-Vis spectroscopy.

The stability of compounds **2a** was studied using UV-Vis spectroscopy. Electronic spectra were obtained in the UV-Vis range (from 200 nm to 800 nm) using a scan rate of 4800.00 nm min⁻¹ using an Agilent Technologies® Cary 60 UV-Vis spectrophotometer with quartz cuvettes with 10 mm path length and 1.0 mL volume. The spectra were recorded at times 0, 24 h, 48 h, and 72 h to visualize the absorption profile of **2a** and determine its stability in phosphate-buffered saline (PBS) with DMSO (0.5%) and pH 7.4, kept in a CO₂ incubator (5%) and at 37 °C, simulating the experimental conditions to which the cells were subjected. The concentration of **2a** was 25 μmol L⁻¹ (v:v).

4. Conclusions

In summary, this paper showed the facile and inexpensive synthesis of six novel In(III) sulfonyldithiocarbamate complexes from their parental dithiocarbamate anions and In(NO₃)₃. These complexes were obtained with 38% to 98% yield and in near-instantaneous reaction times. Complexation was attested by (i) FTIR – hypsochromic shift of ν C=N to 1443.8(19.2) cm⁻¹ and bathochromic shift of ν_{as} CS₂ to 951.2(16.6) cm⁻¹ –, (ii) HRMS – relative error of 0.39(35) between experimental and theoretical m/z values –, and (iii) NMR – δ C=N 207.5(2.81) ppm. Interestingly, statistical analysis of NMR data for 72 homoleptic sulfonyldithiocarbamate complexes in the literature revealed a strong dependence between δ C=N and the d-electron count of the metal cation, for which higher electron counts yielded smaller chemical shifts likely due to increased shielding by π back-bonding.

Analysis of the complexes revealed isomer formation based on different coordination modes – viz., SS-SS, SS-SN, and SN-SN – and, while the experiments alluded to a preponderance of the SS-SS isomer, DFT calculations showed smaller energies for this isomer than the others – $-\Delta\Delta G_{SN-SN} = 8.05(21)$ kcal mol⁻¹ and $\Delta\Delta G_{SN-SS} = 4.28(1.21)$ kcal mol⁻¹. These calculations also showed decreasing $\Delta\Delta G_{SN-SS}$ values according to halogen size. This can be attributed to a greater delocalization of the HOMO orbitals of **2a–b** as the halogen size increases. The ΔG calculations yielded equilibrium constants, K_{eq} , ranging from 90.64 kcal mol⁻¹ to 25031.2 kcal mol⁻¹, supporting the preponderance of the SS-SS isomer. Moreover, ¹³C chemical shift calculations for the C=N corroborated the prevalence of the SS-SS isomer, suggested by the experimental results. Specifically, while the ¹³C δ is 215.0(2.3) ppm for the SS-coordinated ligand, it is 231.4(5) ppm for the SN-coordinated. Compared to the experimental values – viz., 207.5(2.81) ppm –, the SS coordination mode is more plausible.

All complexes were highly active against colorectal adenocarcinoma (HCT-116) cells and moderately active against melanoma (SK-MEL-28) and breast adenocarcinoma (MCF-7) cells. The complexes displayed IC₅₀ values between 3.02(21) μmol L⁻¹ and 5.36(42) μmol L⁻¹ for HCT-116 (IC₅₀ = 2.570(1) μmol L⁻¹ for doxorubicin). All compounds showed substantial selectivity, given the high IC₅₀ values for HaCaT cells (>100 μmol L⁻¹, compared to 0.280(1) μmol L⁻¹ for doxo-

rubicin). In general, the aromatic complexes were less active than the aliphatic, and the cytotoxicity of the latter complexes increased with the halogen size and decreased for the iodine analog. Although further studies regarding the mechanism of action are needed, which are being made, an interplay between (i) the degree of halogen bonds, (ii) steric hindrance, and (iii) the lipophilicity of the dithiocarbamate portion is likely key to differentiate between the analogs.

The biological activity of the metallic complexes **2a–f** cannot be compared to their precursors **1a–f** given their decomposition after prolonged solvent exposure. Hence, the decomposition product of the potassium dithiocarbamate **1b** was isolated as a single crystal for the first time and analyzed. Crystal data revealed that the decomposition yields a supramolecular structure comprised of dithiocarbamate units interspaced by potassium cations, justifying its insolubility in water.

Author contributions

LRC was responsible for data curation, formal analysis, investigation, validation, visualization, writing – original draft, and writing – review & editing. ASB was responsible for data curation, formal analysis, investigation, methodology, software, validation, visualization, writing – original draft, and writing – review & editing. WMAF, LGV, and TDE were responsible for formal analysis and investigation. SSD, RRMS, and IOC were responsible for data curation, formal analysis, investigation, validation, and visualization. EVF was responsible for data curation, resourcer, and software. RD was responsible for data curation, formal analysis, methodology, resources, software, and visualization. MVS was responsible for conceptualization, formal analysis, funding acquisition, investigation, resources, software, supervision, and visualization. WRR was responsible for software, supervision, and writing – review & editing. ECT was responsible for conceptualization, formal analysis, funding acquisition, investigation, methodology, project administration, resources, supervision, validation, and writing – review & editing.

Conflicts of interest

There are no conflicts to declare.

Data availability

Data supporting this article have been included in the ESI.† Crystallographic data for **1b** has been deposited at the Cambridge Crystallographic Data Center (CCDC) under access number 2433188.†

Acknowledgements

The authors thank the Brazilian Federal Agency for Support and Evaluation of Graduate Education (CAPES), the Research

Support Foundation of the State of Minas Gerais (FAPEMIG), and the National Council for Scientific and Technological Development (CNPq) for financial support. They also thank the Federal University of Itajubá (UNIFEI), the Federal University of Minas Gerais (UFMG), and the Federal University of Paraíba (UFPB). They also thank the Laboratory of High-Resolution Nuclear Magnetic Resonance (LAREMAR) in UFMG and the Federal University of Viçosa (UFV) for the NMR analyses. The authors also acknowledge the free-of-charge availability of the ORCA package for academic purposes.

References

- 1 D. Karati, K. R. Mahadik, P. Trivedi and D. Kuma, Alkylating Agents, the Road Less Traversed, Changing Anticancer Therapy, *Anti-Cancer Agents Med. Chem.*, 2022, **22**, 1478–1495, DOI: [10.2174/1871520621666210811105344](#).
- 2 L. Wang, Q. Jiang, S. Chen, S. Wang, J. Lu, X. Gao, D. Zhang and X. Jin, Natural epidithiodiketopiperazine alkaloids as potential anticancer agents: Recent mechanisms of action, structural modification, and synthetic strategies, *Bioorg. Chem.*, 2023, **137**, 106642, DOI: [10.1016/j.bioorg.2023.106642](#).
- 3 A. M. P. Romani, Cisplatin in cancer treatment, *Biochem. Pharmacol.*, 2022, **206**, 115323, DOI: [10.1016/j.bcp.2022.115323](#).
- 4 M. Pourmadadi, M. M. Eshaghi, M. Shaghagi, S. S. Das, R. Arshad, S. Ghotekar, A. Rahdarf, A. L. E. Manicum and S. Pandey, Nano-scale drug delivery systems for carboplatin: A comprehensive review, *OpenNano*, 2023, **13**, 100175, DOI: [10.1016/j.onano.2023.100175](#).
- 5 A. C. Hangan, A. Turza, R. L. Lucaciu, B. Sevastre, E. Páll, L. S. Oprean and G. Borodi, New Cu²⁺ Complexes with N-Sulfonamide Ligands: Potential Antitumor, Antibacterial, and Antioxidant Agents, *Molecules*, 2022, **27**, 3338, DOI: [10.3390/molecules27103338](#).
- 6 D. A. Guk, O. O. Krasnovskaya and E. K. Beloglazkina, Coordination compounds of biogenic metals as cytotoxic agents in cancer therapy, *Russ. Chem. Rev.*, 2021, **90**, 1566, DOI: [10.1070/RCR5016](#).
- 7 R. Paprocka, M. Wiese-Szadkowska, S. Janciauskiene, T. Kosmalski, M. Kulik and A. Helmin-Basa, Latest developments in metal complexes as anticancer agents, *Coord. Chem. Rev.*, 2022, **452**, 214307, DOI: [10.1016/j.ccr.2021.214307](#).
- 8 R. L. Lucaciu, A. C. Hangan, B. Sevastre and L. S. Oprean, Metallo-drugs in cancer therapy: Past, present and future, *Molecules*, 2022, **27**, 6485, DOI: [10.3390/molecules27196485](#).
- 9 U. Ndagi, N. Mhlango and M. E. Soliman, Metal complexes in cancer therapy - An update from drug design perspective, *Drug Des., Dev. Ther.*, 2017, **2017**, 599–616, DOI: [10.2147/DDDT.S119488](#).
- 10 E. S. Pena, L. M. Lifshits, M. Eckshtain-Levi, E. M. Bachelder and K. M. Ainslie, Metal-organic coordination polymers for delivery of immunomodulatory agents, and infectious disease and cancer vaccines, *Wiley Interdiscip. Rev.: Nanomed. Nanobiotechnol.*, 2023, **15**, e1877, DOI: [10.1002/wnan.1877](#).
- 11 C. Riccardi and M. L. Piccolo, Metal-based complexes in cancer, *Int. J. Mol. Sci.*, 2023, **24**, 7289, DOI: [10.3390/ijms24087289](#).
- 12 M. E. Moghadam, M. Rezaeisadat, H. Mansouri-Torshizi, S. Hosseinzadeh and H. Daneshyar, New anticancer potential Pt complex with tertamyl dithiocarbamate ligand: Synthesis, DNA targeting behavior, molecular dynamic, and biological activity, *J. Mol. Liq.*, 2023, **379**, 121651, DOI: [10.1016/j.molliq.2023.121651](#).
- 13 P. A. Ajibade, A. A. Fatokun and F. P. Andrew, Synthesis, characterization and anti-cancer studies of Mn(II), Cu(II), Zn(II) and Pt(II) dithiocarbamate complexes - crystal structures of the Cu(II) and Pt(II) complexes, *Inorg. Chim. Acta*, 2020, **504**, 119431, DOI: [10.1016/j.ica.2020.119431](#).
- 14 E. A. Abdalrazaq, A. Abu-Yamin, D. Taher, A. E. Hassan and A. Elhenawy, Zn(II) and Cd(II) complexes of dithiocarbamate ligands: synthesis, characterization, anticancer, and theoretical studies, *J. Sulfur Chem.*, 2024, **45**, 714–739, DOI: [10.1080/17415993.2024.2384751](#).
- 15 P. F. Chan, K. P. Ang and R. Hamid, Cytotoxicity of bismuth (III) dithiocarbamate derivatives by promoting a mitochondrial-dependent apoptotic pathway and suppressing MCF-7 breast adenocarcinoma cell invasion, *J. Biol. Inorg. Chem.*, 2024, **29**, 217–241, DOI: [10.1007/s00775-023-02041-x](#).
- 16 R. A. Castro, M. R. L. Oliveira, M. M. M. Rubinger, C. H. M. Lima and M. S. Rocha, Platinum Dithiocarbimates as Potential Candidates for Drug Development: Interactions with Double-Stranded DNA, *SSRN*, 2024, DOI: [10.2139/ssrn.4791213](#).
- 17 J. Janczak, M. M. M. Rubinger, L. C. Alves and M. R. L. Oliveira, Poly[di-μ-aqua-[μ₆-N-(4-bromophenylsulfonyl)dithiocarbimato]dipotassium] and poly[di-μ-aqua-[μ₄-N-(4-iodophenylsulfonyl)dithiocarbimato]dipotassium], *Acta Crystallogr., Sect. C: Cryst. Struct. Commun.*, 2012, **68**, m312–m316, DOI: [10.1107/S0108270112040589](#).
- 18 R. S. Amim, M. R. L. Oliveira, G. J. Perpétuo, J. Janczak, L. D. L. Miranda and M. M. M. Rubinger, Syntheses, crystal structure and spectroscopic characterization of new platinum(II)dithiocarbimato complexes, *Polyhedron*, 2008, **27**, 1891–1897, DOI: [10.1016/j.poly.2008.02.030](#).
- 19 M. R. L. Oliveira and V. M. de Bellis, Preparation of novel cobalt(III) complexes with dithiocarbimates derived from sulfonamides, *Transition Met. Chem.*, 1999, **24**, 127–130, DOI: [10.1023/A:1006945923839](#).
- 20 J. Perils, F. Cortezon-Tamarit, N. Kuganathan, G. Kociok-Köhn, J. R. Dilworth and S. I. Pascu, Novel rhenium(V) nitride complexes with dithiocarbamate ligands - A synchrotron X-ray and DFT structural investigation, *Inorg. Chim. Acta*, 2018, **475**, 142–149, DOI: [10.1016/j.ica.2017.11.023](#).

- 21 L. R. Carvalho, L. G. Venturelli, T. C. Lopes, E. V. Filho, V. G. S. Fontenelle, G. F. de Lima, L. L. Y. Visconte and E. d. C. Tavares, Tetraphenylphosphonium Allyldithiocarbimides: A Novel Safe Amine Class of Morita–Baylis–Hillman-Derived NBR Vulcanization Accelerators, *ACS Sustainable Chem. Eng.*, 2023, **11**, 14507–14517, DOI: [10.1021/acssuschemeng.3c03586](#).
- 22 A. C. de Freitas, R. C. L. Machado, F. B. Miguez, M. F. Venâncio, R. Diniz, J. F. Lopes, E. d. C. Tavares and F. B. De Sousa, Electronic and thermodynamic study of Indium(III) complex with *N*-ethyl-sulfonyldithiocarbamate, *J. Mol. Struct.*, 2021, **1237**, 130364, DOI: [10.1016/j.molstruc.2021.130364](#).
- 23 J. G. Gaultney, W. K. Redekop, P. Sonneveld and C. A. Uylde Groot, Novel anticancer agents for multiple myeloma: a review of the evidence for their therapeutic and economic value, *Expert Rev. Anticancer Ther.*, 2014, **12**, 839–854, DOI: [10.1586/era.12.42](#).
- 24 V. Prasad, K. De Jesús and S. Mailankody, The high price of anticancer drugs: origins, implications, barriers, solutions, *Nat. Rev. Clin. Oncol.*, 2017, **14**, 381–390, DOI: [10.1038/nrclinonc.2017.31](#).
- 25 S. K. Singh, R. Chauhan, K. Diwan, M. G. B. Drew, L. Bahadur and N. Singh, Syntheses and structural characterization of new heteroleptic 1,1'-bis(diphenylphosphino) ferrocene-dithio complexes of Ni, Pd and Pt: Their uses as sensitizers in TiO₂ dye sensitized solar cells, *J. Organomet. Chem.*, 2013, **745–746**, 190–200, DOI: [10.1016/j.jorgchem.2013.07.072](#).
- 26 A. E. C. Vidigal, M. M. M. Rubinger, L. F. de Queiroz, L. F. da Silva, L. Zambolim, S. Guilardi, R. A. C. Souza, J. Ellena, E. B. Wetler and M. R. L. Oliveira, Nickel complexes with phosphines and *N*-R-sulfonyldithiocarbimides ligands: New antifungals for the control of *Hemileia vastatrix*, and *Phakopsora pachyrhizi*, *Inorg. Chim. Acta*, 2019, **486**, 724–732, DOI: [10.1016/j.ica.2018.11.037](#).
- 27 A. H. de Oliveira, M. M. M. Rubinger, A. da Silva Rabello, N. M. Albuini-Oliveira, A. E. C. Vidigal, M. R. L. de Oliveira, E. d. C. Tavares and J. E. Serrão, Action of dithiocarbimides salts on the honey bee and its pathogen *Nosema ceranae*, *AMB Express*, 2024, **14**, 82, DOI: [10.1186/s13568-024-01734-z](#).
- 28 N. M. Albuini-Oliveira, M. M. M. Rubinger, A. S. Rabello, E. C. Vidigal, L. L. Y. Visconte, T. C. Lopes and A. L. N. Silva, The influence of ammonium and phosphonium salts on natural rubber vulcanization with experimental and commercial accelerators, *Polym. Bull.*, 2023, **80**, 3717–3743, DOI: [10.1007/s00289-022-04236-9](#).
- 29 C. A. Destefani, L. C. Motta, G. Vanini, L. M. Souza, J. F. A. Filho, C. J. Macrino, E. M. Silva, S. J. Greco, D. C. Endringer and W. Romão, Europium-organic complex as luminescent marker for the visual identification of gunshot residue and characterization by electrospray ionization FT-ICR mass spectrometry, *Microchem. J.*, 2014, **116**, 216–224, DOI: [10.1016/j.microc.2014.05.009](#).
- 30 H.-J. Lee, J.-H. Cha and D.-Y. Jung, Synthesis and crystal structures of mono(2-hydroxyethyl)dithiocarbamate complexes of copper and indium, *J. Mol. Struct.*, 2023, **1275**, 134666, DOI: [10.1016/j.molstruc.2022.134666](#).
- 31 D. P. Dutta, V. K. Jain, A. Knoedler and W. Kaim, Dithiocarbamates of gallium(III) and indium(III): syntheses, spectroscopy, and structures, *Polyhedron*, 2002, **21**, 239–246, DOI: [10.1016/S0277-5387\(01\)00990-1](#).
- 32 E. V. Filho, P. de Sousa Filho, O. Serra, I. Weber, M. Lucena and P. Luz, New luminescent lanthanide-based coordination compounds: Synthesis, studies of optical properties and application as marker for gunshot residues, *J. Lumin.*, 2018, **202**, 89–96, DOI: [10.1016/j.jlumin.2018.05.012](#).
- 33 M. Li, G. M. Ganea, C. Lu, S. L. De Rooy, B. El-Zahab, V. E. Fernand, R. Jin, S. Aggarwal and I. M. Warner, Lipophilic phosphonium–lanthanide compounds with magnetic, luminescent, and tumor targeting properties, *J. Inorg. Biochem.*, 2012, **107**, 40–46, DOI: [10.1016/j.jinorgbio.2011.09.035](#).
- 34 H. Thomadaki, A. Karaliota, C. Litos and A. Scorilas, Enhanced Antileukemic Activity of the Novel Complex 2,5-Dihydroxybenzoate Molybdenum(VI) against 2,5-Dihydroxybenzoate, Polyoxometalate of Mo(VI), and Tetraphenylphosphonium in the Human HL-60 and K562 Leukemic Cell Lines, *J. Med. Chem.*, 2007, **50**, 1316–1321, DOI: [10.1021/jm0610797](#).
- 35 L. M. Gomes Cunha, M. M. Magalhães Rubinger, J. R. Sabino, L. L. Y. Visconte and M. R. Leite Oliveira, Syntheses, crystal structure and spectroscopic characterization of bis(dithiocarbamate)-nickel(II)-complexes: A new class of vulcanization accelerators, *Polyhedron*, 2010, **29**, 2278–2282, DOI: [10.1016/j.poly.2010.04.026](#).
- 36 C. M. Breneman and K. B. Wiberg, Determining atom-centered monopoles from molecular electrostatic potentials. The need for high sampling density in formamide conformational analysis, *J. Comput. Chem.*, 1990, **11**, 361–373, DOI: [10.1002/jcc.540110311](#).
- 37 C. P. Gordon, C. Raynaud, R. A. Andersen, C. Copéret and O. Eisenstein, Carbon-13 NMR Chemical Shift: A Descriptor for Electronic Structure and Reactivity of Organometallic Compounds, *Acc. Chem. Res.*, 2019, **52**, 2278–2289, DOI: [10.1021/acs.accounts.9b00225](#).
- 38 Y. S. Tan, C. I. Yeo, E. R. T. Tiekink and P. J. Heard, Dithiocarbamate Complexes of Platinum Group Metals: Structural Aspects and Applications, *Inorganics*, 2021, **9**, 60, DOI: [10.3390/inorganics9080060](#).
- 39 S. D. Oladipo, B. Omondi and C. Mocktar, Co(III) *N,N'*-diaryl-formamidinium dithiocarbamate complexes: Synthesis, characterization, crystal structures and biological studies, *Appl. Organomet. Chem.*, 2020, **34**, e5610, DOI: [10.1002/aoc.5610](#).
- 40 J. O. Adeyemi, D. C. Onwudiwe and M. Singh, Synthesis, characterization, and cytotoxicity study of organotin(IV) complexes involving different dithiocarbamate groups, *J. Mol. Struct.*, 2019, **1179**, 366–375, DOI: [10.1016/j.molstruc.2018.11.022](#).

- 41 A. Z. Halimehjani, V. Amani, F. Naseri and B. Notash, Synthesis and characterization of metal dithiocarbamate derivatives of (S₁)-1-phenyl-1,2,3,4-tetrahydroisoquinoline, *Sci. Rep.*, 2024, **14**, 29718, DOI: [10.1038/s41598-024-81589-3](https://doi.org/10.1038/s41598-024-81589-3).
- 42 M. R. L. Oliveira, V. M. De Bellis and N. G. Fernandes, Preparation and X-Ray crystal structure of a Novel Nickel (II) complex with dithiocarbamate, *Struct. Chem.*, 1997, **8**, 205–209, DOI: [10.1007/BF02263508](https://doi.org/10.1007/BF02263508).
- 43 M. R. L. Oliveira and V. M. D. Bellis, Preparation of novel cobalt(III) complexes with dithiocarbamates derived from sulfonamides, *Transition Met. Chem.*, 1999, **24**, 127–130, DOI: [10.1023/A:1006945923839](https://doi.org/10.1023/A:1006945923839).
- 44 N. Singh, B. Singh, S. K. Singh and M. G. B. Drew, Syntheses, crystal structures and properties of sterically congested heteroleptic complexes of group 10 metal ions with p-tolylsulfonyl dithiocarbamate and 1,2-bis (diphenylphosphino) ethane, *Inorg. Chem. Commun.*, 2010, **13**, 1451–1454, DOI: [10.1016/j.inoche.2010.08.014](https://doi.org/10.1016/j.inoche.2010.08.014).
- 45 S. K. Singh, M. G. B. Drew and N. Singh, Self assembly of homoleptic Ni(II) dithiocarbamates and dithiocarbamates via Ni...H-C anagostic and C-H... π (chelate) interactions, *CrystEngComm*, 2013, **15**, 10255–10265, DOI: [10.1039/C3CE41358F](https://doi.org/10.1039/C3CE41358F).
- 46 A. A. Oliveira, M. R. L. Oliveira, M. M. M. Rubinger, E. L. Piló, D. C. Menezes and L. Zambolim, Bis(4-fluorophenylsulfonyldithiocarbimato)zincate(II) salts: new antifungals for the control of *Botrytis*, blight, *Quim. Nova*, 2015, **38**, 757–761, DOI: [10.5935/0100-4042.20150075](https://doi.org/10.5935/0100-4042.20150075).
- 47 F. C. Bottega, M. R. L. Oliveira, V. P. Sérvulo, L. L. Y. Visconte, J. D. Ardisson and M. M. M. Rubinger, Syntheses and characterization of novel organometallic tin(IV) complexes with dithiocarbimates and their action as accelerators in the nitrile rubber vulcanization, *Quim. Nova*, 2016, **39**, 801–806, DOI: [10.5935/0100-4042.20160084](https://doi.org/10.5935/0100-4042.20160084).
- 48 F. C. Bottega, M. R. L. Oliveira, M. M. M. Rubinger, C. R. Bellato, J. D. Ardisson and L. Zambolim, Tetraphenylphosphonium and tris (1.10-phenanthroline) iron(II) salts of anionic complexes of dibutyltin(IV) with dithiocarbimates: synthesis, characterization and antifungal activity, *Quim. Nova*, 2016, **39**, 554–560, DOI: [10.5935/0100-4042.20160064](https://doi.org/10.5935/0100-4042.20160064).
- 49 R. A. Castro, M. R. L. Oliveira, J. Janczak and M. M. M. Rubinger, Syntheses and characterization of novel heteroleptic nickel complexes with dithiocarbimates and trithiocarbimates, *Inorg. Chim. Acta*, 2017, **462**, 195–203, DOI: [10.1016/j.ica.2017.03.028](https://doi.org/10.1016/j.ica.2017.03.028).
- 50 N. M. Albuini-Oliveira, M. M. M. Rubinger, A. S. Rabello, E. C. Vidigal, L. L. Y. Visconte, T. C. Lopes and A. L. N. Silva, The influence of ammonium and phosphonium salts on natural rubber vulcanization with experimental and commercial accelerators, *Polym. Bull.*, 2023, **80**, 3717–3743, DOI: [10.1007/s00289-022-04236-9](https://doi.org/10.1007/s00289-022-04236-9).
- 51 R. S. Amim, M. R. L. Oliveira, J. Janczak, M. M. M. Rubinger, L. M. M. Vieira, L. C. Alves and L. Zambolim, Syntheses, characterization, crystal structure and antifungal activity of four tetraphenylphosphonium bis(N-R-sulfonyldithiocarbimato)zincate(II) salts, *Polyhedron*, 2011, **30**, 683–689, DOI: [10.1016/j.poly.2010.12.003](https://doi.org/10.1016/j.poly.2010.12.003).
- 52 S. K. Singh, K. Diwan, M. G. B. Drew and N. Singh, Monometallic salts derived from complex anions of group 10 metal ions with p-tolylsulfonyldithiocarbamate ligand: Synthesis, characterization and properties, *Inorg. Chim. Acta*, 2012, **384**, 176–183, DOI: [10.1016/j.ica.2011.11.055](https://doi.org/10.1016/j.ica.2011.11.055).
- 53 K. Diwan, R. Chauhan, S. K. Singh, B. Singh, M. G. B. Drew, L. Bahadur and N. Singh, Light harvesting properties of some new heteroleptic dithiocarbamate-diamine/diimine complexes of Ni, Pd and Pt studied as photosensitizer in dyesensitized TiO₂ solar cells, *New J. Chem.*, 2013, **38**, 97–108, DOI: [10.1039/C3NJ00507K](https://doi.org/10.1039/C3NJ00507K).
- 54 M. M. S. de Arruda, L. M. G. Cunha, L. L. Y. Visconte, M. M. M. Rubinger, M. R. L. Oliveira and E. B. A. V. Pacheco, Behavior of zinc complex of bis(N-phenylsulfonyldithiocarbamate) as accelerator in the vulcanization of nitrile rubber compounds, *J. Appl. Polym. Sci.*, 2019, **136**, 47211, DOI: [10.1002/app.47211](https://doi.org/10.1002/app.47211).
- 55 R. S. Amim, M. R. L. Oliveira, J. Amim and V. M. De-Bellis, Synthesis and characterization of gold(III) complexes with dithiocarbimates derived from sulfonamides, *Transition Met. Chem.*, 2006, **31**, 1071–1074, DOI: [10.1007/s11243-006-0111-4](https://doi.org/10.1007/s11243-006-0111-4).
- 56 F. C. Bottega, M. R. L. Oliveira, C. V. Garcia, D. C. Menezes, M. M. M. Rubinger and L. Zambolim, Syntheses, characterization and antifungal activity of tris (1,10-phenanthroline)iron(II) bis(n-r-sulfonyldithiocarbimate)zincate(ii), *Quim. Nova*, 2013, **36**, 803–807, DOI: [10.1590/S0100-40422013000600011](https://doi.org/10.1590/S0100-40422013000600011).
- 57 M. R. L. Oliveira, R. Diniz, V. M. De Bellis and N. G. Fernandes, Nickel(II) complexes of dithiocarbimates from sulfonamides: syntheses and crystal structures, *Polyhedron*, 2003, **22**, 1561–1566, DOI: [10.1016/S0277-5387\(03\)00265-1](https://doi.org/10.1016/S0277-5387(03)00265-1).
- 58 B. Singh, M. G. B. Drew, G. Kociok-Kohn, K. C. Molloy and N. Singh, Unprecedented coordination of dithiocarbamate in multinuclear and heteroleptic complexes, *Dalton Trans.*, 2010, **40**, 623–631, DOI: [10.1039/C0DT00582G](https://doi.org/10.1039/C0DT00582G).
- 59 N. Singh, B. Singh, K. Thapliyal and M. G. B. Drew, Synthesis, X-ray crystal structures and properties of complex salts and sterically crowded heteroleptic complexes of group 10 metal ions with aromatic sulfonyl dithiocarbimates and triphenylphosphine ligand, *Inorg. Chim. Acta*, 2010, **363**, 3589–3596, DOI: [10.1016/j.ica.2010.07.065](https://doi.org/10.1016/j.ica.2010.07.065).
- 60 M. R. L. Oliveira, J. E. J. C. Graúdo, N. L. Speziali and V. M. De Bellis, Synthesis of a Novel Nickel(II) Complex with Dithiocarbamate from Sulfonamide, *Struct. Chem.*, 1999, **10**, 41–45, DOI: [10.1023/A:1022018028224](https://doi.org/10.1023/A:1022018028224).
- 61 L. C. Alves, M. M. M. Rubinger, R. H. Lindemann, G. J. Perpétuo, J. Janczak, L. D. L. Miranda, L. Zambolim and M. R. L. Oliveira, Syntheses, crystal structure, spectro-

- scopic characterization and antifungal activity of new *N*-R-sulfonyldithiocarbamate metal complexes, *J. Inorg. Biochem.*, 2009, **103**, 1045–1053, DOI: [10.1016/j.jinorgbio.2009.04.018](#).
- 62 M. R. L. Oliveira, H. P. Vieira, G. J. Perpétuo, J. Janezak and V. M. De Bellis, Syntheses, crystal structure and spectroscopic characterization of novel *N*-R-sulfonyldithiocarbamate and triphenylphosphine nickel(II) complexes, *Polyhedron*, 2002, **21**, 2243–2250, DOI: [10.1016/S0277-5387\(02\)01176-2](#).
- 63 E. de Faria Franca, M. R. L. Oliveira, S. Guillard, R. P. de Andrade, R. H. Lindemann, J. Amim, J. Ellena, V. M. De Bellis and M. M. M. Rubinger, Preparation, crystal structure and spectroscopic characterization of nickel(II) complexes with dithiocarbamate derivated of sulfonamides, *Polyhedron*, 2006, **25**, 2119–2126, DOI: [10.1016/j.poly.2005.11.035](#).
- 64 G. J. Perpétuo, M. R. L. Oliveira, J. Janczak, H. P. Vieira, F. F. Amaral and V. M. De Bellis, Syntheses, crystal structure and spectroscopic characterization of novel *N*-R-sulfonyldithiocarbamate zinc(II) complexes, *Polyhedron*, 2003, **22**, 3355–3362, DOI: [10.1016/j.poly.2003.08.003](#).
- 65 V. Gowda, R. S. Laitinen, V.-V. Telkki, A.-C. Larsson, O. N. Antzutkin and P. Lantto, DFT calculations in the assignment of solid-state NMR and crystal structure elucidation of a lanthanum(III) complex with dithiocarbamate and phenanthroline, *Dalton Trans.*, 2016, **45**, 19473–19484, DOI: [10.1039/C6DT03705D](#).
- 66 E. Martinez-Viviente, P. S. Pregosin and M. Tschoerner, ¹³C NMR of Pd-aryl complexes. Chemical shifts and Pd π -back-bonding, *Magn. Reson. Chem.*, 2000, **38**, 23–28, DOI: [10.1002/\(SICI\)1097-458X\(200001\)38:1<23::AID-MRC606>3.0.CO;2-X](#).
- 67 A. Comas-Vives and J. N. Harvey, How Important Is Back-bonding in Metal Complexes Containing N-Heterocyclic Carbenes? Structural and NBO Analysis, *Eur. J. Inorg. Chem.*, 2011, **2011**, 5025–5035, DOI: [10.1002/ejic.201100721](#).
- 68 A. S. Rabello, M. M. M. Rubinger, L. F. da Silva, A. H. de Oliveira, J. E. Serrão, N. M. Albuini-Oliveira, E. d. C. Tavares, A. E. C. Vidigal, M. R. L. de Oliveira, L. Zambolim, R. A. C. Souza, S. Guillard and J. Ellena, Zinc-dithiocarbamates for the control of *Hemileia vastatrix*: a versatile alternative, *Pest Manage. Sci.*, 2022, **78**, 4741–4752, DOI: [10.1002/ps.7094](#).
- 69 L. C. Dias, M. M. Rubinger, J. P. Barolli, J. D. Ardisson, I. C. Mendes, G. M. de Lima, L. Zambolim and M. R. Oliveira, Syntheses, crystal structure, spectroscopic characterization and antifungal activity of novel dibutylbis (*N*-R-sulfonyldithiocarbamate)stannate(IV) complexes, *Polyhedron*, 2012, **47**, 30–36, DOI: [10.1016/j.poly.2012.08.037](#).
- 70 E. E. Brossard and S. A. Corcelli, Molecular Mechanism of Ligand Binding to the Minor Groove of DNA, *J. Phys. Chem. Lett.*, 2023, **14**, 4583–4590, DOI: [10.1021/acs.jpcclett.3c00635](#).
- 71 G. S. Khan, A. Shah, M. Z. Ur Rheman and D. Barker, Chemistry of DNA minor groove binding agents, *J. Photochem. Photobiol., B*, 2012, **115**, 105–118, DOI: [10.1016/j.jphotobiol.2012.07.003](#).
- 72 M. Feizi-Dehghan, E. Dehghanian and H. Mansouri-Torshizi, DNA/BSA binding affinity studies of new Pd(II) complex with S-S and N-N donor mixed ligands via experimental insight and molecular simulation: Preliminary antitumor activity, lipophilicity and DFT perspective, *J. Mol. Liq.*, 2021, **344**, 117853, DOI: [10.1016/j.molliq.2021.117853](#).
- 73 J. O. Adeyemi, D. C. Onwudiwe, A. C. Ekennia, C. P. Anokwuru, N. Nundkumar, M. Singh and E. C. Hosten, Synthesis, characterization and biological activities of organotin(IV) dialkylthiocarbamate complexes, *Inorg. Chim. Acta*, 2019, **485**, 64–72, DOI: [10.1016/j.ica.2018.09.085](#).
- 74 G. Cavallo, P. Metrangolo, R. Milani, T. Pilati, A. Priimagi, G. Resnati and G. Terraneo, The Halogen Bond, *Chem. Rev.*, 2016, **116**, 2478–2601, DOI: [10.1021/acs.chemrev.5b00484](#).
- 75 B. S. Kitawat and M. Singh, Synthesis, characterization, antibacterial, antioxidant, DNA binding and SAR study of a novel pyrazine moiety bearing 2-pyrazoline derivatives, *New J. Chem.*, 2014, **38**, 4290–4299, DOI: [10.1039/C4NJ00594E](#).
- 76 F. Arjmand, S. Khursheed, T. Roisnel and H. R. Siddique, Copper(II)-based halogen-substituted chromone antitumor drug entities: Studying biomolecular interactions with ct-DNA mediated by sigma hole formation and cytotoxicity activity, *Bioorg. Chem.*, 2020, **104**, 104327, DOI: [10.1016/j.bioorg.2020.104327](#).
- 77 A. Kazimir, T. Götze, P. Lönnecke, B. Murganić, S. Mijatović, D. Maksimović-Ivanić and E. Hey-Hawkins, Exploring Raloxifene-Based Metallodrugs: A Versatile Vector Combined with Platinum(II), Palladium(II) and Nickel(II) Dichlorides and Carborates against Triple-Negative Breast Cancer, *ChemMedChem*, 2024, **19**, e202400006, DOI: [10.1002/cmdc.202400006](#).
- 78 V. A. Blatov, M. O'Keeffe and D. M. Proserpio, Vertex-, face-, point-, Schläfli-, and Delaney-symbols in nets, polyhedra and tilings: recommended terminology, *CrystEngComm*, 2010, **12**, 44–48, DOI: [10.1039/B910671E](#).
- 79 M. O'Keeffe, M. A. Peskov, S. J. Ramsden and O. M. Yaghi, The Reticular Chemistry Structure Resource (RCSR) Database of, and Symbols for, Crystal Nets, *Acc. Chem. Res.*, 2008, **41**, 1782–1789, DOI: [10.1021/ar800124u](#).
- 80 F. Neese and J. Wiley, The ORCA program system, *Wiley Interdiscip. Rev.: Comput. Mol. Sci.*, 2012, **2**, 73–78, DOI: [10.1002/WCMS.81](#).
- 81 F. Neese, Software update: The ORCA program system—Version 5.0, *Wiley Interdiscip. Rev.: Comput. Mol. Sci.*, 2022, **12**, e1606, DOI: [10.1002/WCMS.1606](#).
- 82 P. Sinha, S. E. Boesch, C. Gu, R. A. Wheeler and A. K. Wilson, Harmonic vibrational frequencies: Scaling factors for HF, B3LYP, and MP2 methods in combination with correlation consistent basis sets, *J. Phys. Chem. A*, 2004, **108**, 9213–9217, DOI: [10.1021/JP048233Q](#).

- 83 J. P. Merrick, D. Moran and L. Radom, An evaluation of harmonic vibrational frequency scale factors, *J. Phys. Chem. A*, 2007, **111**, 11683–11700, DOI: [10.1021/jp073974n](https://doi.org/10.1021/jp073974n).
- 84 A. P. Scott and L. Radom, Harmonic Vibrational Frequencies: An Evaluation of Hartree-Fock, Møller-Plesset, Quadratic Configuration Interaction, Density Functional Theory, and Semiempirical Scale Factors, *J. Phys. Chem.*, 1996, **100**, 16502–16513, DOI: [10.1021/jp960976r](https://doi.org/10.1021/jp960976r).
- 85 C. Lee, W. Yang and R. G. Parr, Development of the Colle-Salvetti correlation-energy formula into a functional of the electron density, *Phys. Rev. B: Condens. Matter Mater. Phys.*, 1988, **37**, 785, DOI: [10.1103/PhysRevB.37.785](https://doi.org/10.1103/PhysRevB.37.785).
- 86 F. Weigend and R. Ahlrichs, Balanced basis sets of split valence, triple zeta valence and quadruple zeta valence quality for H to Rn: Design and assessment of accuracy, *Phys. Chem. Chem. Phys.*, 2005, **7**, 3297–3305, DOI: [10.1039/B508541A](https://doi.org/10.1039/B508541A).
- 87 F. Weigend, Accurate Coulomb-fitting basis sets for H to Rn, *Phys. Chem. Chem. Phys.*, 2006, **8**, 1057–1065, DOI: [10.1039/B515623H](https://doi.org/10.1039/B515623H).
- 88 S. Grimme, J. Antony, S. Ehrlich and H. Krieg, A consistent and accurate ab initio parametrization of density functional dispersion correction (DFT-D) for the 94 elements H-Pu, *J. Chem. Phys.*, 2010, **132**, 154104, DOI: [10.1063/1.3382344](https://doi.org/10.1063/1.3382344).
- 89 S. Grimme, S. Ehrlich and L. Goerigk, Effect of the damping function in dispersion corrected density functional theory, *J. Comput. Chem.*, 2011, **32**, 1456–1465, DOI: [10.1002/JCC.21759](https://doi.org/10.1002/JCC.21759).
- 90 F. Neese, An improvement of the resolution of the identity approximation for the formation of the Coulomb matrix, *J. Comput. Chem.*, 2003, **24**, 1740–1747, DOI: [10.1002/JCC.10318](https://doi.org/10.1002/JCC.10318).
- 91 F. Weigend, Accurate Coulomb-fitting basis sets for H to Rn, *Phys. Chem. Chem. Phys.*, 2006, **8**, 1057–1065, DOI: [10.1039/B515623H](https://doi.org/10.1039/B515623H).
- 92 M. Cossi, N. Rega, G. Scalmani and V. Barone, Energies, structures, and electronic properties of molecules in solution with the C-PCM solvation model, *J. Comput. Chem.*, 2003, **24**, 669–681, DOI: [10.1002/JCC.10189](https://doi.org/10.1002/JCC.10189).
- 93 Rigaku Oxford Diffraction, O. Shekha, J. Liu, R. A. Fischer and C. Wöll, CrysAllis PRO, Version 1.171.42.49, 2022, First released in 2011, Rigaku Corporation, Oxford, UK.
- 94 O. V. Dolomanov, L. J. Bourhis, R. J. Gildea, J. A. K. Howard and H. Puschmann, OLEX2: a complete structure solution, refinement and analysis program, *J. Appl. Crystallogr.*, 2009, **42**, 339–341, DOI: [10.1107/S0021889808042726](https://doi.org/10.1107/S0021889808042726).
- 95 G. M. Sheldrick, Crystal Structure Refinement with SHELXL, *Acta Crystallogr., Sect. C: Struct. Chem.*, 2015, **71**, 3–8, DOI: [10.1107/S2053229614024218](https://doi.org/10.1107/S2053229614024218).
- 96 J. L. Farrugia, ORTEP-3 for Windows – a version of ORTEP-III with a Graphical User Interface (GUI), *J. Appl. Crystallogr.*, 1997, **30**, 565, DOI: [10.1107/S0021889897003117](https://doi.org/10.1107/S0021889897003117).
- 97 V. A. Blatov, A. P. Shevchenko and D. M. Proserpio, Applied Topological Analysis of Crystal Structures with the Program Package ToposPro, *Cryst. Growth Des.*, 2014, **14**, 3576–3586, DOI: [10.1021/cg500498k](https://doi.org/10.1021/cg500498k).
- 98 T. Mosmann, Rapid colorimetric assay for cellular growth and survival: application to proliferation and cytotoxicity assays, *J. Immunol. Methods*, 1983, **65**, 55–63, DOI: [10.1016/0022-1759\(83\)90303-4](https://doi.org/10.1016/0022-1759(83)90303-4).
- 99 P. Kumar, A. Nagarajan and P. D. Uchil, Analysis of Cell Viability by the MTT Assay, *Cold Spring Harb. Protoc.*, 2018, **2018**, 095505, DOI: [10.1101/pdb.prot095505](https://doi.org/10.1101/pdb.prot095505).
- 100 R. C. Ferreira, Y. M. Nascimento, P. B. A. Loureiro, R. X. Martins, M. E. S. Maia, D. F. Farias, J. F. Tavares, J. C. R. Gonçalves, M. S. Silva and M. V. Sobral, Chemical Composition, In Vitro Antitumor Effect, and Toxicity in Zebrafish of the Essential Oil from *Conyza bonariensis*, (L.) Cronquist (Asteraceae), *Biomolecules*, 2023, **13**, 1439, DOI: [10.3390/biom13101439](https://doi.org/10.3390/biom13101439).
- 101 S. S. Duarte, D. K. F. Silva, T. M. H. Lisboa, R. G. Gouveia, C. C. N. De Andrade, V. M. De Sousa, R. C. Ferreira, R. O. De Moura, J. N. S. Gomes, P. M. Da Silva, F. L. A. A. De Azevedo, T. S. L. Keesen, J. C. R. Gonçalves, L. M. Batista and M. V. Sobral, Apoptotic and antioxidant effects in HCT-116 colorectal carcinoma cells by a spiro-acridine compound, AMTAC-06, *Pharmacol. Rep.*, 2022, **74**, 545–554, DOI: [10.1007/s43440-022-00357-0](https://doi.org/10.1007/s43440-022-00357-0).